

Partition of Unity Extension of Functions on Complex Domains

Fredrik Fryklund^{a,*}, Erik Lehto^a, Anna–Karin Tornberg^a

^a*KTH Mathematics, Swedish e–Science Research Centre,
100 44 Stockholm, Sweden*

Abstract

We introduce an efficient algorithm, called partition of unity extension or PUX, to construct an extension of desired regularity of a function given on a complex multiply connected domain in $2D$. Function extension plays a fundamental role in extending the applicability of boundary integral methods to inhomogeneous partial differential equations with embedded domain techniques. Overlapping partitions are placed along the boundaries, and a local extension of the function is computed on each patch using smooth radial basis functions; a trivially parallel process. A partition of unity method blends the local extrapolations into a global one, where weight functions impose compact support. The regularity of the extended function can be controlled by the construction of the partition of unity function. We evaluate the performance of the PUX method in the context of solving the Poisson equation on multiply connected domains using a boundary integral method and a spectral solver. With a suitable choice of parameters the error converges as a tenth order method down to 10^{-14} .

Keywords: Function extension, Embedded Domain, Boundary Integral Method, Radial Basis Function, Partition of Unity, Linear Elliptic Partial Differential Equation

1. Introduction

This paper addresses the issue of how to numerically construct an extension of a function defined on a complex domain. Without prior acquaintance with the topic it could appear simple. However, adding requirements on the global regularity of the extended function it becomes a non-trivial task. Furthermore, it is often desirable that the extended function has compact support and that it can be efficiently constructed. One important application for function extension is to extend the applicability of integral equation methods for solving partial differential equations (PDEs). Integral equation methods have been shown to be both highly accurate and efficient when solving homogeneous constant coefficient elliptic partial differential equations in complex geometry. Function extension is a key component in a framework for solving non-homogeneous elliptic PDEs, and furthermore to solve time-dependent equations such as the heat equation and extending from the solution of Stokes equations to Navier-Stokes equations [1, 2, 3].

The idea is to avoid solving the full linear elliptic inhomogeneous PDE, given on a complex domain, by splitting the problem into two. The right-hand side is extended to a geometrically simpler domain, such as a box, and as part of the full solution, a particular solution is computed on this simpler domain. The homogeneous problem is solved on the original domain with modified boundary conditions, such that the total solution is the sum of the two. This general idea has been used also for other numerical methods and this group of methods is often referred to as embedded boundary techniques. For simple geometries an arsenal of powerful solution methods are available, but their accuracy is often limited by the global regularity of the extended function. Several different function extension methods, used in this context, have been suggested in recent years [4, 5, 6, 7, 8, 9].

*Corresponding author

Email addresses: `ffry@kth.se` (Fredrik Fryklund), `e1ehto@kth.se` (Erik Lehto), `akto@kth.se` (Anna–Karin Tornberg)

The approach to function extension suggested by Askham et al. [4] and Stein et al. [6] are both based on the same idea, but quite different in implementation. Given f on a domain $\bar{\Omega}$, use the values of f on the boundary of Ω as the Dirichlet data for the external Laplace problem

$$\Delta w = 0 \text{ in } \mathbb{R}^2 \setminus \Omega, \quad (1)$$

$$w = f \text{ on } \partial\Omega. \quad (2)$$

Then a globally continuous extension f^e of f is given by

$$f^e(\mathbf{y}) = \begin{cases} f(\mathbf{y}), & \mathbf{y} \in \Omega, \\ w(\mathbf{y}), & \mathbf{y} \in \mathbb{R}^2 \setminus \Omega. \end{cases} \quad (3)$$

In [4], this problem is solved by an integral equation based method, whereas in [6] it is coupled with a so called *immersed boundary system of equations*. This extension will be in C^0 , but will not have compact support. To obtain higher regularity the biharmonic equation can be solved instead of (1)–(2), or even polyharmonic. Their respective work show the complexity of the problem and what price is considered reasonable to pay to obtain an extension. Moreover both observe that the accuracy of the solution to the associated PDE relies heavily on the regularity of said extension f^e .

Another alternative, given by [9], is to extend the solution to the PDE, instead of the right hand side, and use an active penalty method. A function extension of global regularity k is created by matching normal derivatives of degree k of the given boundary data. The extension is expressed in a basis that is rapidly decaying with the distance to the boundary. Function extension can also be achieved by Fourier continuation methods: in $1D$ the domain of interest is embedded into a larger one and a smooth periodic extension is constructed, which yields an appropriate setting for spectral methods. Dimensional splitting is used for higher dimensional problems. See [10, 11, 12, 13] and the references therein. The methods and the associated references included above is by no means a complete list of methods for function extension. In all mentioned cases above, no higher than a fourth order method is obtained for solving the Poisson equation.

In this paper, we present a new method, *Partition of Unity Extension*, or PUX, to compute a compactly supported extension of a function. We assume that the values of a function f are known at all points of a regular grid that fall inside a domain Ω , and we want to compute the values of the extended function on this regular grid outside of Ω . The domain Ω can be multiply connected. In the PUX method, overlapping circular partitions or patches are placed along the boundaries such that each is intersected by the boundary $\partial\Omega$ and a local extension is defined on each patch. A second layer of patches is placed outside of the first, on which the local values are defined to be zero. These zero patches enter the definition of the partition of unity function that is used to blend the local extensions into a global one, imposing compact support and regular decay to zero. The choice of functions used to build up the partition of unity function determines the regularity of the extended function.

The local extensions on the patches intersected by $\partial\Omega$ are determined using radial basis functions (RBFs). RBF centres are placed irregularly with the same distribution for each circular patch, and an RBF interpolant is determined via a least squares problem, using the values of f on the regular points inside Ω . The values of the local extension are then computed on the regular points inside the patch that fall outside of Ω . Always centring the patches at grid points of the regular grid, a matrix A can be precomputed once and be used for all patches. For each patch, an identification is made of which points are inside and outside Ω and a local least squares problem with the relevant rows of A is solved with the inside data, a trivially parallel task.

To assess the quality of a function extension it must be considered in its context of use, as there is no unique extension over the boundary of a domain. In this paper, we use it to solve the Poisson equation, using an integral equation approach. Thus the results by Askham et al. in [4] are suitable for comparison.

The paper is organised as follows: in section 2 we detail how we solve the Poisson equation assuming an extension of the right hand side f is known. In section 3 we introduce the concepts and techniques from RBF interpolation and

the partition of unity method that we need to introduce our method. The PUX method is presented in section 4, where a function extension is constructed. Thereafter follows section 5 with a discussion of sources of errors associated with function extension and solving the Poisson equation. Section 6 is a summary, combined with implementation details, for solving the Poisson equation with the techniques described in this paper. In section 7 we perform numerical experiments and carefully discuss parameter choices. Finally our conclusions and an outlook are presented in section 8.

2. The Poisson equation on irregular domains in a boundary integral method environment

To understand why a function extension is useful for solving linear elliptic PDEs, and why its construction is motivated to pursue, we sketch the solution procedure. Consider the Poisson equation with Dirichlet boundary conditions, stated as

$$\Delta u = f \text{ in } \Omega, \quad (4)$$

$$u = g \text{ on } \partial\Omega, \quad (5)$$

where Ω is a simply or multiply connected compact domain in \mathbb{R}^2 with a Lipschitz continuous boundary, meaning corners but not cusps are allowed. We will refer to the Poisson equation as the full problem. Introduce homogeneous and particular solutions u^H and u^P such that $u = u^H + u^P$. Let B be a simple box domain of size $[-L, L]^2$ which embeds Ω , and let E be the complement of $\bar{\Omega}$ relative B . We refer to E as the *extension domain*. If we know an extension f^e of f from Ω to B , such that $f^e = f$ in Ω and $\text{supp}(f^e) \subset B$, the particular solution u^P can be computed from

$$\Delta u^P = f^e \text{ in } \mathbb{R}^2, \quad (6)$$

$$u^P \in L^2(\mathbb{R}^2), \quad (7)$$

assuming f^e can be constructed numerically, which is the focus of this paper. The homogeneous solution u^H is obtained by solving the Laplace equation with modified Dirichlet boundary conditions, i.e.

$$\Delta u^H = 0 \text{ in } \Omega, \quad (8)$$

$$u^H = g - u^P|_{\partial\Omega} \text{ on } \partial\Omega. \quad (9)$$

The numerical treatment of the Laplace equation on Ω is discussed in subsection 2.1. It can be solved for the homogeneous solution to high precision very effectively with a boundary integral method. In our specific setting, the Dirichlet boundary data will be modified according to the solution of the free-space Poisson equation (6), as given in (9). If the extension f^e of f is known and has compact support one can truncate the free-space Poisson equation (6)–(7) to a box; then a numerical solution can efficiently be obtained by fast spectral methods, as described in 2.2. Therefore it is imperative f^e has high global regularity. Note that both (6)–(7) and (8)–(9) are relatively simple problems to solve numerically to high accuracy at a low computational cost, if said extension f^e is simple to construct. The solution to the full problem (4)–(5) is given $u = u^H + u^P$.

2.1. Homogeneous solution

Consider the Dirichlet problem for the Laplace equation,

$$\Delta u^H = 0 \text{ in } \Omega, \quad (10)$$

$$u^H = \tilde{g} \text{ on } \partial\Omega, \quad (11)$$

with Ω assumed to be simply connected for now. The numerical solution to a linear elliptic homogeneous PDEs is attractive to compute using a boundary integral method, as it can be both accurate and efficient. The boundary integral formulation becomes more dense if expressed with a complex representation, which is natural to adopt since we consider the plane \mathbb{R}^2 . The use of complex notation will be isolated for treating (10)–(11) and all expressions have an equivalent counterpart in \mathbb{R}^2 . We will move freely between the two representations as we see fit. In \mathbb{C} points will be

denoted τ and z , and the real and imaginary parts of any $\tau \in \mathbb{C}$ are denoted $\text{Re}\{\tau\}$ and $\text{Im}\{\tau\}$.

By introducing an unknown density $\mu : \partial\Omega \rightarrow \mathbb{R}$ the solution u^H of (10)–(11) can be represented with a double layer potential

$$u^H(z) = \frac{1}{2\pi} \int_{\partial\Omega} \mu(\tau) \text{Im} \left\{ \frac{d\tau}{\tau - z} \right\}, \quad \forall z \in \Omega. \quad (12)$$

Clearly it is sufficient to know μ on the boundary $\partial\Omega$ to have an expression for u^H anywhere in Ω . Thus only $\partial\Omega$ needs to be discretised and the dimensionality of (10)–(11) has been reduced by one. To obtain the unknown density function μ we treat (12) in the sense of a Cauchy principal value as we pass the limit $z \rightarrow z_0$ for $z \in \Omega$ and apply the boundary condition. This yields

$$\tilde{g}(z_0) = \frac{1}{2}\mu(z_0) + \frac{1}{2\pi} \int_{\partial\Omega} \mu(\tau) \text{Im} \left\{ \frac{d\tau}{\tau - z_0} \right\}, \quad z_0 \in \partial\Omega. \quad (13)$$

The integrand has a well-defined limit as $\tau \rightarrow z_0$. This is a Fredholm integral equation of second kind. If $\partial\Omega$ is Lipschitz continuous the integrand is a *compact* integral operator, thus the Fredholm alternative states that (13) is uniquely solvable for μ [14]. This property is inherited by the discretised system, which is obtained by dividing the boundary $\partial\Omega$ into panels of equal length and on each apply the 16 points *Gauss–Legendre quadrature rule*. The total number of Gauss–Legendre panels is denoted $N_{\partial\Omega}$. We use Nyström’s method, meaning the collocation points are set to coincide with the quadrature points z_j , with $j = 1, \dots, 16 N_{\partial\Omega}$. The resulting linear system is

$$\tilde{g}(z_i) = \sum_{\substack{j=1 \\ j \neq i}}^{16 N_{\partial\Omega}} \mu(z_j) \omega_j \text{Im} \left\{ \frac{\tau'_i}{\tau_i - z_j} \right\} + \mu(z_i) \left(\omega_j \text{Im} \left\{ \frac{\tau''_i}{\tau'_i} \right\} + \frac{1}{2} \right), \quad i = 1, 2, \dots, 16 N_{\partial\Omega}, \quad (14)$$

with ω_j denoting quadrature weights. Here τ'_i and τ''_i mean that the boundary $\partial\Omega$ has been parametrised as $\tau = \tau(t)$ and differentiated at t_i once and twice, respectively. The corresponding matrix–vector representation of (14) yields a dense system matrix. A property of the discretisation of a second kind integral equation is that the condition number does not increase with finer resolution of $\partial\Omega$. We solve for μ at the quadrature points with *GMRES*.

Once μ is known, u^H can be computed at the points z in Ω of interest by evaluating a numerical approximation of the integral in (12). The integrand, however, becomes nearly singular for z close to $\partial\Omega$, which causes a loss of accuracy if the regular panel based 16 point Gauss–Legendre rule is used. This can to some extent be remedied by increasing the number of panels along $\partial\Omega$, as in Figure 1 where the centre image has twice as many panels as the left. Since the error increases exponentially fast as the boundary is approached [15], this can not provide accurate solutions arbitrarily close to the boundary. Excellent results can however be obtained by applying special quadrature techniques.

We use one such technique, namely an interpolatory quadrature method introduced by Ojala and Helsing [16]. This method is based on expanding the complex density μ as a polynomial in the complex variable τ over one panel and invoking recursive formulas to analytically evaluate all integrals that are needed. The coefficients of the polynomial are the solution of a Vandermonde system. It is however possible to solve the transposed problem instead, for which the right hand side depends only on the panel geometry and the location of the evaluation point, and not on the discrete values of μ on the panel. Together with a scaling and rotation of the panel, this controls the ill-conditioning of the problem.

If an evaluation point is within a panel length from a panel’s midpoint, we check if the special quadrature method needs to be invoked. Here, we use one of the above mentioned analytically known integrals from expanding μ and check the accuracy in the numerically obtained value (with the Gauss–Legendre quadrature rule) for this integral. It contains the same near singularity as (12) and is a good indicator of the accuracy that will be obtained by the regular quadrature.

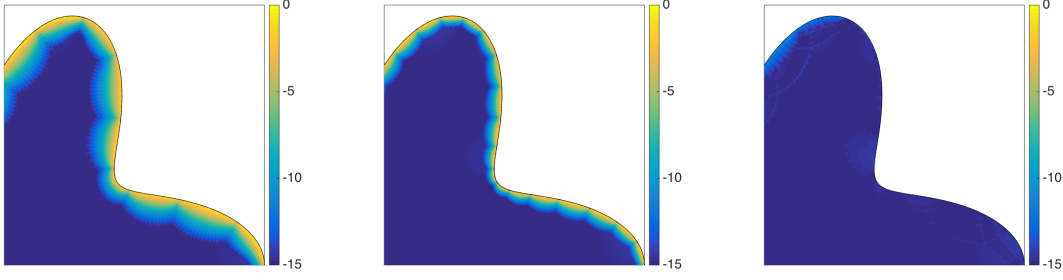


Figure 1: Example of pointwise relative error, in \log_{10} -scale, in part of the computational domain when solving the Laplace equation using: normal quadrature using 35 panels (left), normal quadrature using 70 panels (centre) and special quadrature using 35 panels (right).

So far only simply connected domains have been considered. To fix notation for the Laplace equation on multiply connected domains, let Ω consist of a finite $(\kappa + 1)$ -connected region with a boundary $\partial\Omega$ consisting of $(\kappa + 1)$ closed curves. These are denoted $\partial\Omega_0, \partial\Omega_1, \dots, \partial\Omega_\kappa$, where $\partial\Omega_0$ forms the outer boundary of the region Ω . Let the *cavity* Ω_k be the set enclosed by $\partial\Omega_k$, disjoint with Ω , for $k = 1, 2, \dots, \kappa$. For such a setting the associated integral equation to (12) has a nontrivial nullspace; consequently the Fredholm alternative is not applicable. Thus modifications to the method described above are in order. We apply the remedy suggested in [17] and the references therein. Instead of (12), the solution to Laplace equation on multiply connected domains is

$$u^H(z) = \frac{1}{2\pi} \int_{\partial\Omega} \mu(\tau) \operatorname{Im} \left\{ \frac{d\tau}{\tau - z} \right\} + \sum_{k=1}^{\kappa} A_k \log |z - z_k|, \quad \forall z \in \Omega, \quad (15)$$

where z_k is an interior point of Ω_k , and the coefficients A_k and the density μ are unknown. By imposing

$$\int_{\partial\Omega_k} \mu(\tau) d|\tau| = 0, \quad \text{for } k = 1, 2, \dots, \kappa \quad (16)$$

where integration is due to arc length, the resulting boundary integral equation

$$\begin{cases} \tilde{g}(z_0) = \frac{1}{2}\mu(z_0) + \frac{1}{2\pi} \int_{\partial\Omega} \mu(\tau) \operatorname{Im} \left\{ \frac{d\tau}{\tau - z_0} \right\} + \sum_{k=1}^{\kappa} A_k \log |z_0 - z_k|, & z_0 \in \partial\Omega. \\ \int_{\partial\Omega_k} \mu(\tau) d|\tau| = 0, & \text{for } k = 1, 2, \dots, \kappa. \end{cases} \quad (17)$$

satisfies the Fredholm alternative. Hence the coefficients A_k and the density μ can be solved for simultaneously via (17). Observe that the special quadrature techniques for evaluating (15) are the same as for the simply connected case, as the points z_k are chosen so that $\log |z - z_k|$ pose no numerical difficulties to evaluate.

While not necessary to solve the Laplace equation, a useful aspect of (12) is that for $\mu \equiv 1$ one has

$$\frac{1}{2\pi} \int_{\partial\Omega} \operatorname{Im} \left\{ \frac{d\tau}{\tau - z} \right\} = \begin{cases} 1, & \text{if } z \in \Omega, \\ 1/2, & \text{if } z \in \partial\Omega, \\ 0, & \text{if } z \notin \bar{\Omega}. \end{cases} \quad (18)$$

Thus the framework for solving the Laplace equation can be used to identify points as in Ω , on the boundary of Ω or outside $\bar{\Omega}$.

2.2. Particular solution

The particular solution to the full problem (4)–(5) is acquired by solving the free-space Poisson equation (6)–(7). A key component is an extension f^e of f ; its construction with PUX is described in section 4. If f^e is known, such that $f^e = f$ in Ω and $\text{supp}(f^e) \subset B$, the solution to (6)–(7) is known to be

$$u^P(\mathbf{x}) = \int_{\mathbb{R}^2} K(\|\mathbf{x} - \mathbf{y}\|_2) f^e(\mathbf{y}) d\mathbf{y} = \int_B K(\|\mathbf{x} - \mathbf{y}\|_2) f^e(\mathbf{y}) d\mathbf{y}, \quad (19)$$

where K is the Green's function. In \mathbb{R}^2 one has

$$K(r) = \frac{-1}{2\pi} \log(r). \quad (20)$$

For a derivation see any basic textbook on the subject, e.g. [18]. To handle (19) numerically we apply the approach suggested by Vico et al. in [19]: since f^e has compact support in B , the Green's function can be truncated without changing the value of $u^P(\mathbf{x})$ in (19) for $\mathbf{x} \in B$. Replace K with

$$\tilde{K}(r) = \begin{cases} \frac{-1}{2\pi} \log(r) & \text{for } r < R = \frac{3}{2}L, \\ 0 & \text{otherwise,} \end{cases} \quad (21)$$

where $[-L, L]^2$ is the box B containing $\text{supp}(f)$; $3/2L$ is slightly larger than the greatest possible distance between two points in B . Denote the Fourier transform of \tilde{K} as $\hat{\tilde{K}}$, which has a closed analytical expression, namely

$$\hat{\tilde{K}}(k) = \frac{1 - J_0(Rk)}{k^2} - \frac{R \log(R) J_1(Rk)}{k}, \quad (22)$$

where J_0 and J_1 are the Bessel functions of the first kind of order 0 and 1, respectively. Here $k = \|\mathbf{k}\|_2$ with $\mathbf{k} \in \mathbb{R}^2$, thus it is radial. Furthermore, the limit as k goes to 0 is well-defined:

$$\lim_{k \rightarrow 0} \hat{\tilde{K}}(k) = \frac{R^2}{4} (1 - 2 \log(R)). \quad (23)$$

The Fourier coefficients for u^P are

$$\hat{u}^P(\mathbf{k}) = \hat{\tilde{K}}(k) \hat{f}^e(\mathbf{k}), \quad \mathbf{k} \in \mathbb{R}^2, \quad (24)$$

and the solution $u^P(\mathbf{x})$ is given by the inverse Fourier transform

$$u^P(\mathbf{x}) = \frac{1}{(2\pi)^2} \int_{\mathbb{R}^2} \hat{u}^P(\mathbf{k}) e^{i\mathbf{k} \cdot \mathbf{x}} d\mathbf{k}. \quad (25)$$

Clearly it is beneficial to have $\hat{\tilde{K}}(k)$ instead of $\hat{K}(k) = -1/k^2$, which has a singularity at $k = 0$. The integral in (25) can be discretised with the trapezoidal rule, which allows the usage of an inverse FFT to compute it. It will be sufficiently resolved in k -space if upsampling of the FFT is done with a factor greater or equal to $5/2$ for $R = 3/2L$ [20]. Hence, to numerically obtain u^P on a uniform grid in B we apply FFTs to transform the values of f^e and \tilde{K} given on a uniform grid. The FFTs are zero padded to obtain the required upsampling, and an inverse FFT is applied after multiplication of the coefficients (25). This zero padding avoids pollution from periodic copies of the truncated kernel, and can be reduced to a factor of two after a precomputation step for $\hat{\tilde{K}}$, see [19]. This is the standard minimum oversampling to compute an aperiodic convolution. This yields an FFT based method for the free-space Poisson equation that converges spectrally as the uniform grid over B is refined, if f^e is smooth.

To solve the full problem (4)–(5) the solution u^P is needed on $\partial\Omega$ to define the modified boundary conditions for the Laplace equation (8)–(9). A non-uniform FFT with the Fourier coefficients \hat{u}^P obtained above allows us to evaluate u^P on $\partial\Omega$ [21].

3. Background for interpolation with RBFs and partition of unity methods

The PUX–method is based on the structure of interpolation with radial basis functions (RBFs) and partition of unity methods. This section aims to present a comprehensive background for these techniques, before the function extension is discussed in section 4. An informal description of RBFs and partition of unity methods for the interpolation problem can be summarised as follows. The interpolation domain Ω is covered with overlapping partitions. On each partition a local interpolant, based on f , is constructed with RBFs. These are combined into a global interpolant via a weighted sum, where the weights sum to 1 everywhere in Ω .

3.1. Radial basis functions

First we cover interpolation through collocation with RBFs for some general data set. Then we discuss the somewhat more involved least squares approach, which is the one we will apply. To interpolate over a set of scattered data with a collocation approach, we set each data point to be the centre for an RBF and enforce known function values at these points. This results in a linear system we solve to obtain interpolation weights. Once solved for we can evaluate the interpolant at other desired locations.

To be more precise: Let $s_{f,\Omega}$ be the interpolant of $f \in C^k(\Omega)$ on the domain $\Omega \subset \mathbb{R}^2$ such that

$$s_{f,\Omega}(\mathbf{y}) = \sum_{j=1}^M \lambda_j \varphi_j(\mathbf{y}), \quad (26)$$

where $\varphi_j(\mathbf{y}) = \varphi(\|\mathbf{y} - \mathbf{x}_j\|_2)$ is the RBF centred at \mathbf{x}_j and \mathbf{y} is some point in \mathbb{R}^2 . RBFs are univariate functions from \mathbb{R}_+ to \mathbb{R} , where $\mathbb{R}_+ = \{x \in \mathbb{R} \mid x \geq 0\}$, that disregard geometry. Thus they are mesh free by construction. Given an RBF it forms a basis for the local approximation space $\mathcal{N}_\varphi(\Omega)$ referred to in the literature as the *native Hilbert space*. Its nature depends on the RBF of choice, for more details see [22].

One option to obtain the unknown *interpolation coefficients* $\lambda_j \in \mathbb{R}$ is by collocation at the RBF centres, i.e. for $\mathbf{x}_i \in \{\mathbf{x}_j\}_{j=1}^M$ we require $f(\mathbf{x}_i) = \sum_{j=1}^M \lambda_j \varphi_j(\mathbf{x}_i)$. This is equivalent to solving

$$\Phi \Lambda = F \quad (27)$$

for $\Lambda = \{\lambda_j\}_{j=1}^M$, where $\Phi = \{\varphi_i(\mathbf{x}_j)\}_{i,j=1}^M$ and $F = \{f_j\}_{j=1}^M$ with $f_j = f(\mathbf{x}_j)$. The method for obtaining the coefficients through solving (27) with Gaussian–elimination will be referred to as *RBF–Direct*.

An RBF φ is said to be *positive definite* if the resulting interpolation matrix Φ is positive definite. The matrix Φ is symmetric due to the nature of RBFs. There is a plethora of positive definite RBFs and we consider only such functions.

Associated with certain RBFs is the *shape parameter* $\varepsilon \in \mathbb{R}_+$, which sets the flatness of the RBF. Let $r = \|\mathbf{y} - \mathbf{x}_j\|_2$ and consider for example the *Gaussian*

$$\varphi(r) = e^{-(\varepsilon r)^2}, \quad (28)$$

for which $\mathcal{N}_\varphi(\Omega)$ is a subset in the Sobolev space $W_2^m(\Omega)$ for any m . A function f is an element of $\mathcal{N}_\varphi(\Omega)$ for a given ε if the square root of its Fourier transform decays faster than the Fourier transform of (28). For further reading see [22]. As ε goes to zero, the RBF becomes increasingly flat and consequently the columns in Φ become increasingly linearly dependent. Thus the condition number of Φ grows and the weights $\{\lambda_j\}_{j=1}^M$ become large and oscillatory. However, these are purely numerical effects since the RBFs do indeed form the basis for an approximation space with nice properties. In fact, the accuracy of the approximation increases as ε goes to zero [23], but this effect may not be discernible due to high condition numbers, see Figure 2. The appropriate range for ε is problem dependent and no general optimal value can be chosen, although according to theory the smaller ε the smaller the error in infinite precision.

Regularity	$\varphi(r)$
$C^{0,1}$	$(1-r)_+^2(2+r)$
$C^{0,2}$	$(1-r)_+^3(8+9r+3r^2)$
$C^{2,3}$	$(1-r)_+^4(4+16r+12r^2+3r^3)$
$C^{2,4}$	$(1-r)_+^5(8+40r+48r^2+25r^3+5r^4)$
$C^{4,5}$	$(1-r)_+^6(6+36r+82r^2+72r^3+30r^4+5r^5)$

Table 1: Wu functions with compact support in $r \in [0, 1)$ in $C^{k,\tilde{k}}$: k is the regularity at origin and \tilde{k} is the regularity at the edge of the support. They are positive definite up to \mathbb{R}^3 . Furthermore $(\cdot)_+ = \max(0, \cdot)$.

Apart for Gaussians other common choices are different compactly supported RBFs, such as the so called *Wu* functions. In the literature Wu functions are tabulated after their order of regularity at origin, see for example [24] and Table 1. In our application the regularity at the boundary of the support is of larger interest, where it tends to be greater. This will become apparent in subsequent sections. Thus we will denote the space of continuous functions of regularity k at the origin, but \tilde{k} at the edge of the support, as $C^{k,\tilde{k}}$.

Given a compactly supported RBF of regularity $2k$ at origin the corresponding native Hilbert space is the Sobolev space $W_2^{\frac{d}{2}+k+\frac{1}{2}}(\Omega)$, with $\Omega \subset \mathbb{R}^2$ [25]. If the compact support is small enough they yield a sparse structure for Φ . However this is a trade-off for accuracy, which increases with support size [24]. We will return to the choice between global and local RBFs.

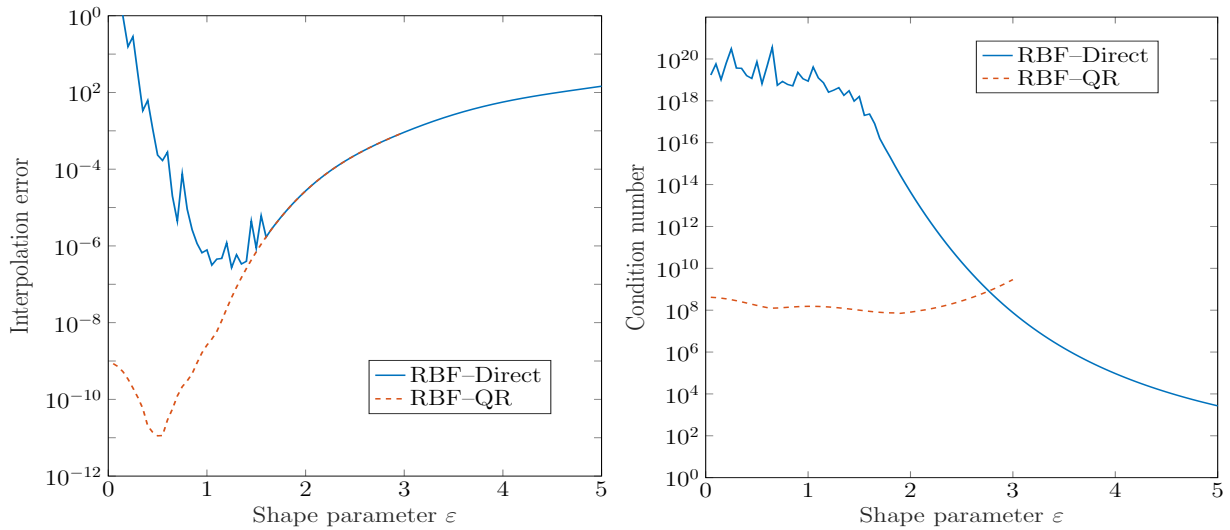


Figure 2: Illustration of typical interpolation problem for RBF-Direct for $\varepsilon \in (0, 5]$ and RBF-QR for $\varepsilon \in (0, 3]$. Left: interpolation error. Right: condition number of Φ .

As mentioned above, the ill-conditioning of Φ as the shape parameter ε goes to zero is a purely numerical effect and it can be partially circumvented by replacing RBF-Direct with stable methods, such as *RBF-QR*. This paper does not aim to fully explain the RBF-QR algorithm, instead we refer to [23] for details. The main idea is that the approximation space spanned by positive definite RBFs contains good solutions to the interpolation problem (27), therefore a change of basis can remove the ill-conditioning of Φ . This change of basis is accomplished by the RBF-QR algorithm and its positive effects are clear from Figure 2. Note that for large values of ε and large distances between RBF centres

the RBF–QR is neither needed nor worthwhile, and should hence not be used.

As we proceed to the function extension problem, we will have values of f defined on points from a uniform FFT grid. It is a well–known fact in the RBF–community that a uniform point distribution for RBF centres yields a larger condition number. The efficiency of RBF–QR is hampered as well, as it would be limited to collocating at about 100 uniform grid points.

To obtain a more robust and efficient method, we decouple the centres and the data points, and find an interpolant in the least squares sense, as is done in [26]. Consider a non–uniform distribution of M RBF centres at locations $\{\mathbf{x}_j\}_{j=1}^M$, but the values of f given at N uniform point locations $\{\tilde{\mathbf{x}}_i\}_{i=1}^N$. See Figure 3 for a union of uniform data locations and non–uniform RBF centres. We seek an approximation of f at the non–uniform points, that is $F = \{f(\mathbf{x}_j)\}_{j=1}^M$, in order to create an interpolant with non–uniform RBF centres and data like (27). Introduce $\tilde{\Phi} = \{\varphi_j(\tilde{\mathbf{x}}_i)\}_{i,j=1}^{N,M}$ and $\tilde{F} = \{f(\tilde{\mathbf{x}}_i)\}_{i=1}^N$, where $\tilde{\Phi}$ is an $N \times M$ –matrix. Recall that Φ and Λ is of size $M \times M$ and $M \times 1$, respectively. Then, replacing Λ by $\Phi^{-1}F$ from (27), we have

$$\tilde{\Phi}\Lambda = \tilde{F} \Leftrightarrow \tilde{\Phi}\Phi^{-1}F = \tilde{F}, \quad (29)$$

and let $A = \tilde{\Phi}\Phi^{-1}$. Obtaining the unknown F from (29) is a least squares problem and numerically we require that N is sufficiently larger than M to yield good solutions. This approach allows us to use non–uniform RBF centres which significantly improves the stability, but still lets the data be represented on the uniform grid. Furthermore, the ill–conditioning of Φ , associated with the shape parameter ε , is reduced by the use of RBF–QR. The RBF–QR algorithm is intended for a formulation as (29), since it computes A , rather than Φ^{-1} , which acts as a mapping of data from non–uniformly to uniformly distributed locations. With F known we can interpolate to obtain values $F_{\mathbf{y}}$ at some locations $\{\mathbf{y}_k\}_{k=1}^K$ by creating $A_{\mathbf{y}} = \Phi_{\mathbf{y}}\Phi^{-1}$ where $\Phi_{\mathbf{y}} = \{\varphi_j(\mathbf{y}_k)\}_{k,j=1}^{K,M}$; then $F_{\mathbf{y}} = A_{\mathbf{y}}F$ which we set to be $s_{f,\Omega}(\mathbf{y}_k)$ for $k = 1, \dots, K$.

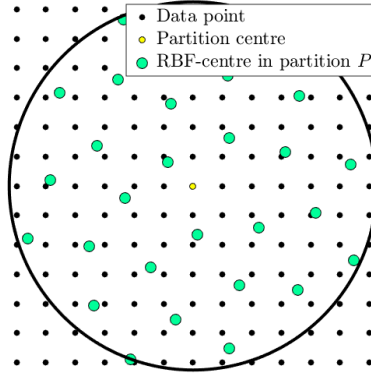


Figure 3: Schematic figure of RBF centres and uniformly distributed data points.

The distribution of non–uniform RBF centres is the same as in [26] and is a *Vogel node* distribution defined as

$$\mathbf{x}_j = \sqrt{\frac{j}{M}} \left(\cos(j\pi(3 - \sqrt{5})), \sin(j\pi(3 - \sqrt{5})) \right), \quad j = 1, \dots, M, \quad (30)$$

and is quasi–uniform. In Figure 3 the 28 mint green dots are Vogel nodes. Such a distribution of RBF centres is near–optimal and the RBF–QR algorithm performs well up to about 400 centres. Recall that in order obtain good

approximations by solving the least squares system N must be sufficiently larger than M .

A drawback when using Gaussians is their global nature and consequently the resulting interpolation matrix Φ is large and dense. An alternative would be to use compactly supported RBFs, but to obtain good approximations their support needs to be large, resulting again in a non-sparse matrix structure. This encourages the implementation of a partition of unity method, which is often used in combination with RBFs. It decouples the size of Φ and the choice of the RBF used for interpolation.

3.2. Partition of Unity

The idea of a partition of unity approach is to combine local approximations s_{f,Ω_i} of the function f on partitions Ω_i , $i = 1, \dots, N_p$. These partitions form the set $\{\Omega_i\}_{i=1}^{N_p}$. They are overlapping and constitute a covering of Ω , meaning

$$\bar{\Omega} \subset \bigcup_{i=1}^{N_p} \bar{\Omega}_i. \quad (31)$$

Associated with this covering we construct a family of compactly supported and continuous functions $\{w_i\}_{i=1}^{N_p}$ such that $\text{supp}(w_i) = \Omega_i$ for every $i = 1, \dots, N_p$ and

$$\sum_{i=1}^{N_p} w_i(\mathbf{y}) \equiv 1, \quad \forall \mathbf{y} \in \bigcup_{i=1}^{N_p} \bar{\Omega}_i. \quad (32)$$

Each weight function w_i corresponds to a partition Ω_i in the covering. They are constructed as a weighted average of compactly supported RBFs which we denote ψ , to distinguish them from the Gaussians φ . This is often referred to in the literature as Shepard's method [27]:

$$w_i(\mathbf{y}) = \frac{\psi_i(\mathbf{y})}{\sum_{j=1}^{N_p} \psi_j(\mathbf{y})}, \quad (33)$$

where $i \in 1, 2, \dots, N_p$. An RBF ψ_i is centred at $\mathbf{p}_i \in \mathbb{R}^2$ and its support defines the associated partition Ω_i . The set $\{\mathbf{p}_i\}_{i=1}^{N_p}$ contains all partition centres.

We will use the same distribution of non-uniform RBF centres for $\{\varphi_j\}_{j=1}^M$ for every partition. Thus the centres $\{\mathbf{x}_j\}_{j=1}^M$ can then be selected for near-optimal approximation properties, where Vogel node distribution is one such example, see (30). The approximation s_f of f on Ω is a weighted sum of the local approximations s_{f,Ω_i} , i.e.

$$s_f(\mathbf{y}) = \sum_{i=1}^{N_p} w_i(\mathbf{y}) s_{f,\Omega_i}(\mathbf{y}) \quad (34)$$

where the local approximations are obtained through interpolation with RBFs:

$$s_{f,\Omega_i}(\mathbf{y}) = \sum_{j=1}^M \lambda_j \varphi_j(\mathbf{y}), \quad (35)$$

see subsection 3.1. From now on we will always use Gaussians as RBFs for interpolation and all partitions are discs. As we proceed with function extension the local approximations are only required for partitions partially in Ω . For partitions entirely in Ω constructing a local extension is redundant, since f is known there.

4. Function extension by PUX

In this section we describe how to construct a compactly supported function extension of high global regularity. To make the description of the PUX-method accessible we will first extend a function with extrapolation, using tools presented in the previous section. For this extension we do not control how f^e approaches zero. Thereafter we apply the full PUX-method to construct a compactly supported function extension with a chosen regularity.

4.1. Extrapolation

For extrapolation of f defined on a bounded and closed domain $\bar{\Omega} \subset \mathbb{R}^2$ the following procedure is used. Partition centres $\{\mathbf{p}_i\}_{i=1}^{N_p}$, i.e. centres for the compactly supported RBFs we denote ψ_i , are distributed uniformly with respect to arc length along the boundary $\partial\Omega$ as in the left image in Figure 4. Each partition centre is associated with a partition for which a local extension is constructed. They are referred to as *extension partitions*. The partition centres are moved to the closest uniform grid point in Ω , such that if all extension partitions have the same radius R_p , a single matrix A from expression (29) can be precomputed and reused for every partition Ω_i to approximate the local interpolants s_{f,Ω_i} , $i = 1, \dots, N_p$. Doing so is vital for the efficiency for PUX, as RBF-QR is required for accuracy but is 10 to 15 times more computationally expensive than RBF-Direct.

We introduce some useful notation: let $\mathbf{y}_E = \{\mathbf{y} \in E\}$ and $\mathbf{y}_\Omega = \{\mathbf{y} \in \Omega\}$, where E is the complement of $\bar{\Omega}$ relative B . Any combination of subindices simply means points in the associated intersection, e.g. $\mathbf{y}_{E,i} = \{\mathbf{y}_E \in \Omega_i\}$. The point distribution between partitions differ only with regard to which points that belong to Ω or E . See Figure 4 and compare with Figure 3; observe that we have RBF centres outside of Ω . For some partition centre \mathbf{p}_i we precompute a single matrix A based on all uniform points and Vogel nodes within distance R_p of the centre. For a given partition Ω_i we identify the uniform points \mathbf{y}_{Ω_i} as belonging to Ω or to E . By simple row manipulation we rewrite (29) as

$$\begin{bmatrix} A_\Omega \\ A_E \end{bmatrix} F = \begin{bmatrix} \tilde{F}_\Omega \\ \tilde{F}_E \end{bmatrix} \quad (36)$$

where the subscripts denote which set the points \mathbf{y}_{Ω_i} belong to. Since \tilde{F}_Ω is known we can solve $A_\Omega F = \tilde{F}_\Omega$ for F in least squares sense. Thus the number of defined interior values for f , i.e. the size of \tilde{F}_Ω , must be greater than the number of RBF-centres, i.e. Vogel nodes, in order to have an overdetermined least squares problem. The *local extension* is computed as

$$s_{f,\Omega_i}(\mathbf{y}_{\Omega_i,E}) = \tilde{F}_E = A_E F. \quad (37)$$

To ease notation we refer to $s_{f,\Omega_i}(\mathbf{y}_{\Omega_i,E})$ as f_i^e when no ambiguity can arise. The global extension f^e is the weighted combination of all local extension evaluated for $\cup_i \mathbf{y}_{\Omega_i,E}$, but for $\cup_i \mathbf{y}_{\Omega_i,\Omega}$ we set $f^e = f$ and $f^e = 0$ otherwise. The extension has compact support, but no means are taken to control how it decays. Hence in most events the extension will be discontinuous over the boundary of its support. A remedy is presented in the following subsection.

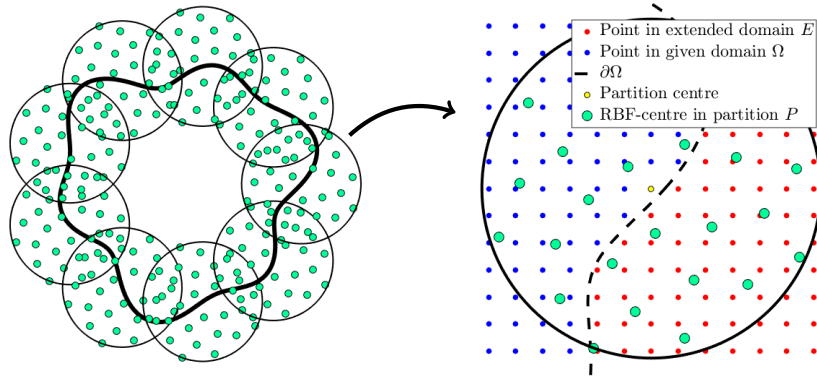
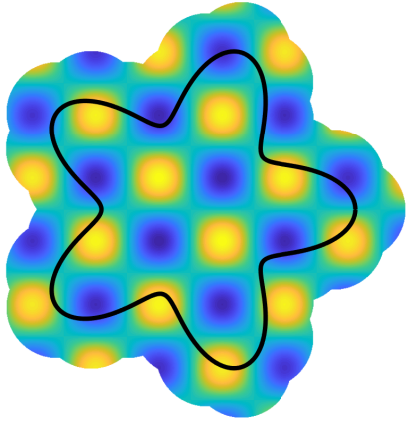
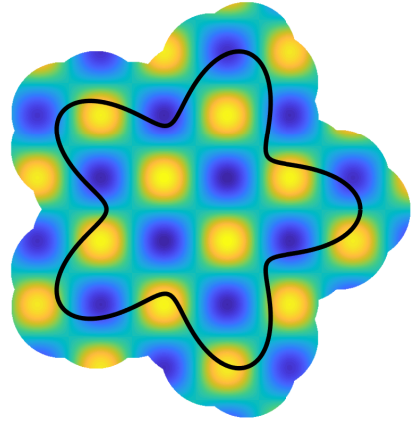


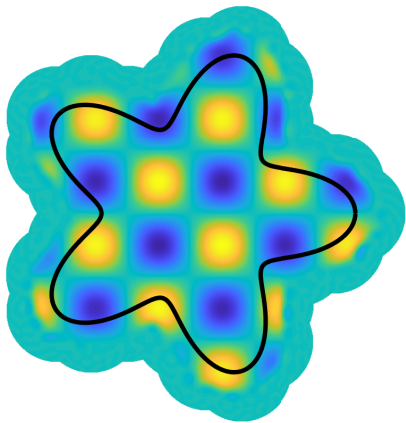
Figure 4: Left: Schematic figure of distribution of extension partitions along $\partial\Omega$ for a complex domain. The green markers correspond to RBF-centres and the distribution is repeated for every partition. Right: Schematic figure of identifying uniformly distributed points as inside or outside Ω .



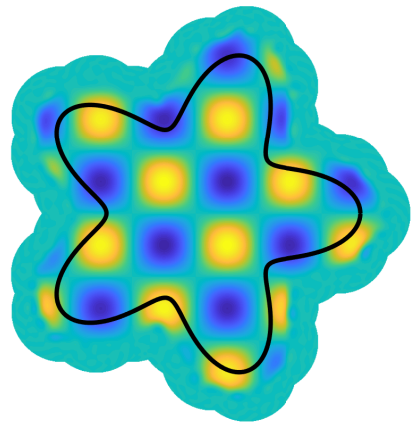
(a) Function f from (46) on starfish shaped domain Ω .



(b) Extrapolation of (46) as in subsection 4.1.



(c) Blended with a layer of zero-partitions, see subsection 4.2.



(d) High regularity function extension f^e with compact support, see (38).

Figure 5: Illustration of various steps of function extension with PUX.

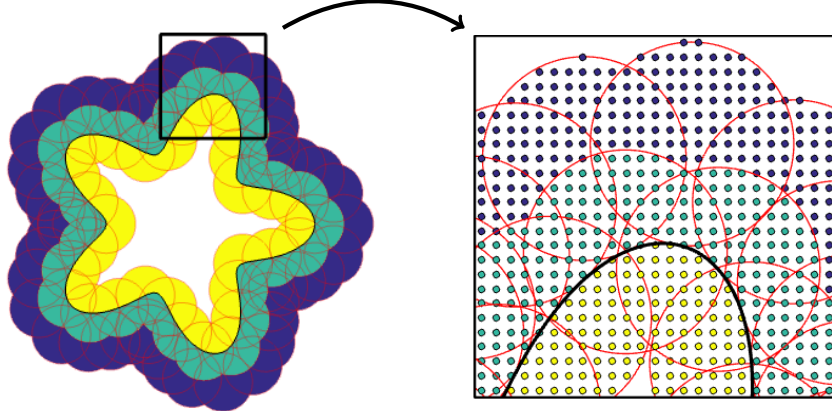


Figure 6: Schematic image for function extension from a star shaped domain Ω given by the black border. Observe that in this figure the partitions are not centred at uniform grid points. The red overlapping circles are the partitions. The yellow section corresponds to the uniform data points used for creating the local extension f_i^e , the blue section to points where $f^e = 0$ and the green sector is a blend of the two.

4.2. Compactly supported function extension

To construct a compactly supported function extension f^e of f , which is continuous or of higher regularity as it is extended by zero outside of its support, we modify the extension obtained in the previous subsection. Yet another layer of partitions is added such that it overlaps the extension partitions. These partitions do not intersect $\bar{\Omega}$ and no interpolation is performed for them. They are referred to as *zero partitions* and the corresponding set is denoted as $\{\Omega_i^0\}_{i=1}^{N_p^0}$. The associated s_{f, Ω_i^0} is set to be identically equal to zero for $i = 1, \dots, N_p^0$.

The weight function in a partition, as defined in (33), is zero at the boundary of the partition. Hence, as the local extension in the first layer of partitions are blended with the zero values in the zero partitions, the global extension that is defined will be forced to zero over the overlapping region. See Figure 5c where the local extensions are suppressed to zero in the overlaps. Hence zero partitions should be placed such that f^e has a controlled decay to zero and that the size of the overlap with extension partitions are about the same. Thus the global extension will in these parts have the same regularity as w , i.e. the compactly supported RBF ψ . Observe that there always is jump over $\partial\Omega$, since an analytical expression is used for points inside Ω and an approximation outside. It is not numerically discernible if the approximation is good enough. However, if poor then f^e is an extension of a poor approximation of f , i.e. another function. This occurs if e.g. the number of RBF-centres per partition is too few. Consequently the jump $\partial\Omega$ will be of such magnitude that f^e will behave as a discontinuous function.

Once f^e is obtained it is extended by zero to a box $B = [-L, L]^2$ that embeds the support of f^e . The expression for a function extension obtained by PUX is

$$f^e(\mathbf{y}) = \begin{cases} f(\mathbf{y}), & \mathbf{y} \in \Omega, \\ \sum_{i=1}^{N_p+N_p^0} w_i(\mathbf{y}) s_{f, \Omega_i}(\mathbf{y}), & \mathbf{y} \in \bigcup_{i=1}^{N_p} \mathbf{y}_{\Omega_i, E}, \\ 0, & \text{otherwise.} \end{cases} \quad (38)$$

The sum also includes the zero partitions to emphasise that the weight functions in extension partitions are affected by them; even though the local values in a zero partition are identically zero. The function f^e evaluated on a uniform grid in B can be used to solve (6)–(7) for the particular solution to the full problem.

5. Sources of numerical errors

Given a function f defined on a bounded domain Ω , there is no unique compactly supported extension to \mathbb{R}^2 . To measure the quality of the function extension obtained by PUX for a set of parameters, we study the numerical solution to the full problem (4)–(5). Consequently, the errors directly associated with PUX cannot be isolated and analysed separately, but we can give an account for sources of numerical errors. In this section we discuss the local interpolation error, the error originating from approximating local interpolants with least squares, errors dependent on the choice of the compactly supported RBF to construct the weight function, errors from using an FFT–solver for the free–space Poisson equation (6) with the truncated Green’s function and errors associated with boundary integral method for solving the Laplace equation (8)–(9).

First we briefly discuss the error from solving the Laplace equation. Assume $\partial\Omega$ is sufficiently resolved with 16 point Gauss–Legendre panels. Then the error associated with the boundary integral method for solving the Laplace equation converges rapidly as the number of Gauss–Legendre panels increases. The resolution of $\partial\Omega$ is chosen a priori based on g , therefore it is important that the modified boundary conditions $g - u^p$ are not much harder to resolve than g . If this is true, then the error associated with the boundary integral method can with efficiency and without difficulty be controlled such that it does not dominate.

Now we turn our attention to the errors connected to function extension and solving the free–space Poisson equation (6). We start with the local interpolation error in some partition Ω_i ; to initially simplify the analysis assume $\{\lambda_j\}$ in (26) is obtained by collocation, i.e. not with least squares. If the RBFs $\{\varphi_j\}$ are Gaussians, then according to [28] the following estimate for the interpolation error holds:

$$\|f - s_{f,\Omega_i}\|_{L_\infty(\bar{\Omega}_i)} \leq 3e^{C \log(h)/\sqrt{h}} \|f\|_{\mathcal{N}_\varphi}, \quad (39)$$

where C is a constant depending on the space dimension, the norm and φ , but not on f or h . Here h is the *fill distance*: the diameter of the largest ball possible to fit between the RBF centres in a partition and thus a measure of the density of the RBF–centres. Further $\|\cdot\|_{\mathcal{N}_\varphi}$ is the norm associated with the native space \mathcal{N}_φ . Although technically only true for $f \in \mathcal{N}_\varphi$ it works well in practise for smooth functions and especially bandlimited functions. For further discussion see [29]. From (39) we conclude that the interpolation error in each partition for collocation converges spectrally as we increase the number of RBF–centres within a partition. We note that the estimate (39) still holds when s_{f,Ω_i} is obtained with least squares, since the same RBFs are used and therefore the approximation space is the same as for collocation [26]. However, this will not be true for the extension.

To understand what happens with the interpolation error when the local interpolants are weighted together with a partition of unity method we need the concept of *regular covering*: Assume that each $\mathbf{y} \in \Omega$ only belongs to a finite number of Ω_i , that each partition contains enough data points to allow a unique interpolant and that each partition Ω_i satisfies an interior cone–condition [30]. A covering $\{\Omega_i\}_{i=1}^{N_p}$ satisfying these requirements is denoted a regular covering. In our applications, these conditions are easily met and we will assume that our coverings are regular.

A remarkable property of partition of unity is that the global approximation order of s_f inherits the local one for s_{f,Ω_i} , under the assumptions that the covering $\{\Omega_i\}_{i=1}^{N_p}$ is regular [30]. This property can be understood intuitively, just consider the following example. Let $\mathbf{y} \in \Omega_1 \cap \Omega_2$ and assume the local approximant is exact up to some tolerance ϵ_i , i.e. $\|f - s_{f,\Omega_i}\|_{L_\infty(\bar{\Omega}_i)} \leq \epsilon_i$ for $i = 1, 2$. Then

$$|f(\mathbf{y}) - s_f(\mathbf{y})| \leq \sum_{i=1}^2 w_i(\mathbf{y}) |f(\mathbf{y}) - s_{f,\Omega_i}(\mathbf{y})| \leq \underbrace{(w_1(\mathbf{y}) + w_2(\mathbf{y}))}_{=1} \max(\epsilon_1, \epsilon_2) \quad (40)$$

and the potential error from low order weight functions is not noticeable, as they form a partition of unity and thus sum to one at every point belonging to a partition. Instead, the global interpolant inherits the local approximation order.

Now we consider the function extension and discuss its regularity and influence on the error, still assuming that the local interpolants are obtained through collocation instead of approximated with least squares. The speed at which the extension goes to zero is controlled by the choice of RBF we use as ψ and on the size of the overlapping region. A smaller region means a more rapid decay, thus a high grid resolution might be required to resolve the extension. Therefore it is preferable, from this point of view, to have as much overlap between extension partitions and zero-partitions as possible, and to have a large partition radius. On the other hand, the extension may not be well-behaved far from the boundary and a greater partition radius requires more RBF-centres to resolve f . The RBF-QR algorithm is not capable of removing ill-conditioning, associated with small values of ε , for A with over 400 RBF centres. Furthermore, the larger the partition radius R_p is the more we lose locality.

Increasing the number of RBF centres does not necessarily increase the accuracy, instead it can make the situation worse. Compare with polynomial interpolation, where a higher order polynomial basis means more oscillations. A similar effect is present for RBF-interpolation. A remedy is to make the partitions smaller, instead of increasing the number of RBF centres. However, this requires a finer resolution of the uniform grid, as smaller partitions implies a shorter span for the extension to go to zero.

Theoretically, things get more complicated when we consider the function extension obtained by least squares. With collocation the interpolant and f would agree on all uniform data locations in Ω , where as for the least squares interpolant, there can be a discrepancy at these points. Defining f^e according to (38), where the original values of f are used inside Ω , there will hence be a discontinuity across $\partial\Omega$ of the size of the error in the least squares interpolant. However, this discontinuity is a technicality, since it can be made arbitrary small by controlling (39). If no such measures are taken the error for solving the full problem decays with second order as the uniform grid is refined. Since A can be precomputed once and used for all partitions, we can set the number of RBF-centres M sufficiently large and make the partitions appropriately small in order not to suffer from a poor approximation of the interpolant due to least squares.

We now discuss the weight functions' influence on the accuracy for numerically solving (4)–(5). The intersection between a zero and an extension partition is the distance over which the weight functions suppress the extension to zero. This implies that a high grid resolution may be required not to resolve f on Ω , but to resolve the suppression to zero over the aforementioned intersection. Further the extension will inherit the regularity of the compactly supported RBF used to create the weights w . Thus we may expect an asymptotic convergence of $4 + \tilde{k}$ for an RBF with regularity $C^{k, \tilde{k}}$; 2 orders for solving the free-space Poisson equation plus $2 + \tilde{k}$ since the \tilde{k} :th derivative has bounded variation [31]. The greater the regularity of the Wu RBF the harder it is to resolve, thus requiring a finer uniform grid. Therefore we will not consider infinitely smooth compactly supported RBFs as weight functions, such as the construction by Ying et al. [32]. In section 7 we show how to optimally choose the regularity \tilde{k} of the compactly supported RBF, given a resolution of the uniform grid on B and partition radius R_p .

Finally we briefly mention errors associated with evaluating the solution to the free-space Poisson equation with a truncated kernel by FFTs and for obtaining u^P on $\partial\Omega$ with non-uniform FFT. Replacing the Green's function K with the truncated Green's function \tilde{K} in (19) involves no approximation. The main source of error is resolving the Fourier transform of \tilde{K} and f^e with FFTs. Given a smooth right hand side f^e the error for solving (6) decays spectrally as the uniform grid is refined, assuming method parameters are set appropriately [19]. Concerning the non-uniform FFT it takes a given tolerance as input argument, and assuming sufficiently many Fourier coefficients are available no greater error than the set tolerance will be introduced.

6. Summary and implementation of entire solution procedure

Guidelines for picking appropriate values for the numerical implementation are given in the next section. In this section the computational procedure for solving the full problem (4)–(5) is summarised, alongside implementation details:

- Discretise $\partial\Omega$ into $N_{\partial\Omega}$ Gauss–Legendre panels, each with 16 Gauss–Legendre points. Set R_p as radius for all extension partitions and let them overlap by slightly more than a radius. This yields a number N_p of extension partitions $\{\Omega_i\}_{i=1}^{N_p}$, with corresponding partition centres $\{\mathbf{p}_i\}_{i=1}^{N_p}$, distributed uniformly with respect to arc length along $\partial\Omega$.
- Let $\Omega \subset B = [-L, L]^2$, which must contain all $\mathbf{y} \in \cup_i \bar{\Omega}_i$, and let E be the complement of $\bar{\Omega}$ relative B . At the locations $E \setminus \cup_i \bar{\Omega}_i$ the extended function will be zero and need not to be included, see (38) or Figure 7. For some N_u construct a uniform grid on B with resolution $2L/N_u$ to be used by the FFT–solver. Sort the N_u^2 uniform grid points as *inside* or *outside* $\bar{\Omega}$. To identify a point \mathbf{y} as belonging to Ω or E , one can evaluate (18) for it.
- Relocate each partition centre \mathbf{p}_i to the closest uniform grid point inside Ω to allow for precomputation of A and to avoid reducing the regularity of f^e by evaluating the RBFs at their origin.
- Pick a compactly supported RBF for ψ to construct the weight functions $\{w_i\}_{i=1}^{N_p+N_p^0}$ with Shepard’s method (33). We use Wu–functions, see Table 1 and choose among them based on \tilde{k} , which denotes the compactly supported RBF’s regularity, with a neighbourhood around the origin excluded. This value sets the regularity of the global extension f^e .
- The shape parameter ε for the Gaussians used as the RBF for interpolation (26) needs to be set. The number of RBF centres M , i.e. Gaussians, inside each partition and which distribution must be specified too. We use a Vogel node distribution (30) and for a given mesh size N_u and partition radius R_p the amount M must be set such that (29) is an overdetermined system. If the partition radius R_p is appropriately small in relation to the curvature of $\partial\Omega$, each partition will contain roughly the same amount of uniform data locations where f is known. This does not only give the same interpolation qualities on each patch, but is a measure to ensure that for each patch the least squares problem (29) is sufficiently overdetermined. In the next section we will give a guide to choosing all aforementioned parameters.
- To precompute the matrix A pick some point on the uniform grid. Within distance R_p of this grid point, find the uniform grid points $\{\tilde{\mathbf{x}}_i\}_{i=1}^N$ and distribute a set of Vogel nodes $\{\mathbf{x}_j\}_{j=1}^M$, see Figure 3. For these points we compute $A = \tilde{\Phi}\Phi^{-1}$ with RBF–Direct, where $\tilde{\Phi} = \{\varphi_j(\tilde{\mathbf{x}}_i)\}_{i,j=1}^{N,M}$ and $\Phi = \{\varphi_j(\mathbf{x}_i)\}_{i,j=1}^{M,M}$, see paragraph above expression (29). If the condition number of Φ is not of moderate size, then A is recomputed with RBF–QR. An open–source implementation in MATLAB for computing A with RBF–QR can be found at [33]. This is done only once, and A is reused for all extension partitions.
- For each partition Ω_i the precomputed matrix A needs to be separated into A_Ω and A_E , as in (36). The patch specific separation depends on which uniform points \mathbf{y}_{Ω_i} that belong to E or Ω . Standard solvers are used to solve the least squares systems, see the paragraph below expression (36), in order to evaluate the local extension f_i^e by (37).
- It is also possible to precompute the local component ψ used for constructing the weight functions (33). As for precomputing A , simply evaluate ψ for all uniform points within distance R_p of some partition centre. These values can be used for all partitions to construct the partition of unity weights.
- The N_p^0 zero partitions must at least overlap the boundary of the union of Ω and the extension partitions in order to have a controlled decay of f^e to zero. One simple way of achieving this is to distribute $N_p^0 = 2N_p$ points uniformly, with respect to arc length, on the boundary. Place the zero–partitions in the normal direction at a distance of R_p from the boundary $\partial\Omega$. Initially their radius is set to R_p , but as they should not intersect $\bar{\Omega}$ rescaling may need to be required. Thus the zero–partitions can have varying radius.

- Combine the local extensions $\{f_i^e\}$ by weight functions to obtain the global extension f^e of f , given by (38), for each point from the uniform grid in B .
- Since f^e has compact support in a box B embedding Ω we can apply the method in [19], as explained in subsection 2.1. Hence we use the precomputed truncated spectral representations of the Green's function (23), to evaluate the solution to (6)–(7) with an FFT, upsampled by a factor of 2. This yields the particular solution u^p on a uniform grid in B and also the Fourier coefficients of u^p . Evaluate u^p at the Gauss–Legendre points given by the Gauss–Legendre panels along $\partial\Omega$ with a non–uniform FFT. The non–uniform FFT we apply is described in [21] and we use their open source library. As input it takes an error tolerance which we set to 10^{-14} . These values are used to obtain the modified boundary conditions $g - u^p$ for (8)–(9).
- With u^p known on the boundary, we can solve (14) numerically with GMRES for μ at the Gauss–Legendre points, as described in subsection 2.1. The required modifications when Ω is a multiply connected domain are given in [17]. Obtaining u^H in Ω is just a matter of post processing, where the special quadrature is applied to points in Ω close to $\partial\Omega$. The final solution to (4)–(5) on a uniform grid in Ω is $u = u^H + u^p$. Note that we are not restricted to evaluating u at these locations. Since the Fourier coefficients \hat{u}^p and the density μ are known we can evaluate u at any point in Ω .

7. Numerical Results

This section is organised as follows. We start with a general discussion of how to set the various parameters. Then a strategy for finding appropriate values is presented, based on experiments for a simple numerical setting. Thereafter this strategy is shown to work also for choosing parameters for more advanced settings. Finally we present some timings to give an idea of the complexity of function extension in relation to solving the free–space Poisson equation.

With the *error* we refer to the relative discrete ℓ_2 error for solving the full problem (4)–(5), measured as

$$\frac{\|\mathbf{u}_{\text{exact}} - \mathbf{u}_{\text{numerical}}\|_{\ell_2}}{\|\mathbf{u}_{\text{exact}}\|_{\ell_2}}, \quad (41)$$

where

$$\|\mathbf{u}\|_{\ell_2} = \sqrt{\sum_{i=1}^{N_{\text{eval}}^2} |u_i|^2 / N_{\text{eval}}^2} \quad (42)$$

for a vector of length N_{eval}^2 . We measure the error on an evaluation grid, which is a problem dependent uniform grid with resolution $2L/N_{\text{eval}}$, where $N_{\text{eval}} = 1000$.

The domains used for numerical experiments are expressed in the complex plane as

$$Re^{(n i \theta)} \left(c_0 + \sum_j (c_j \cos(j\theta) + d_j \sin(j\theta)) \right) + a + ib \quad (43)$$

where $\theta \in [0, 2\pi)$ and n gives the orientation. The non–zero coefficients are stated for each complex multiply connected domain.

To obtain a numerical solution to the full problem (4)–(5) the following parameters need to be set:

- ε : the shape parameter for the Gaussians used as basis for interpolation.
- R_p : partition radius.
- N_u : number of uniform grid points in one spatial direction.

- M : The number of Vogel–nodes (30), i.e. the number of RBF centres per extension partition.
- $N_{\partial\Omega}$: Number of Gauss–Legendre panels. Each panels has 16 Gauss–Legendre points.
- L : Length of the side of the box shaped computational domain B .
- \tilde{k} : The regularity of the compactly supported RBF used to compute the weights (33).

The amount of overlap between partitions also has to be set. We always let them overlap by slightly more than a radius R_p . A large overlap gives the extension f^e a more uniform band around Ω where it decays to zero, which grants a more predictable behaviour. Thus this parameter does not vary for different numerical settings.

In general, the solution is not sensitive to the shape parameter ε , as long as ε is within an appropriate range of values. We use $\varepsilon = 2$ for all numerical experiments in this article. Still, this is a problem dependent variable and may require tuning for substantially different domains and functions than presented in this paper. Observe that the right hand side (46) for example 1 is an element of the native space \mathcal{N}_φ for $\varepsilon = 2$, which is not the case for the right hand sides (49) and (50), corresponding to example 2 and 3.

Another problem dependent parameter is the partition radius R_p . It is strongly related to the grid resolution N_u and the number of RBF centres M , i.e. the number of number of Vogel nodes (30). Recall that the RBF–QR algorithm has limited capacity for M , which is around 400. Thus the greater the variation of f the smaller partitions are required to obtain good approximations for the local interpolants. The choice of M depends on the given f , and will thus be different for each numerical experiment.

There is a simple way to find an appropriate value for R_p and to obtain a range for good choices of ε : measure the residual for solving the least squares problem (29) on some partition. A large residual implies that either ε or R_p needs to be changed. Another indication that smaller partitions are needed is if $\max_{\mathbf{y} \in \mathbf{y}_{\Omega_i, \varepsilon}} |s_{f, \Omega_i}(\mathbf{y})|$ from (37) is significantly larger than $\max_{\mathbf{y} \in \mathbf{y}_{\Omega_i, \Omega}} |f(\mathbf{y})|$ for any partition Ω_i ; the extension should take on values in the same range as f .

By construction f^e decays to zero over a distance of approximately R_p , meaning smaller partitions may require a larger value for N_u to resolve f^e . Thus one may wish to set R_p as large as possible, in order to avoid constructing an f^e much harder to resolve than f . However, in most events N_u is chosen to resolve f^e close to the boundary of its support, not f on Ω . For difficult right hand sides, such as (49) from example 2 and (50) from example 3, the scale is about the same. For simpler functions resolving f^e is clearly harder, see for example (46).

Previously we have said that (29) needs to be overdetermined, but no quantitative measure has been given of how much the solution is improved if more data points \mathbf{y}_{Ω_i} , relative to M , is used. Therefore we introduce the measure

$$\beta_i = \frac{\text{number of data points in partition } \Omega_i}{M}, \quad (44)$$

and $\beta_{\min} = \min_i \beta_i$. It is an useful tool for analysing the relationship, in terms of error, between number of RBF centres M and the available data in an extension partition, which is based on N_u .

The larger \tilde{k} , the higher regularity of f^e and thus faster decay of the Fourier coefficients. But we also need to take into account that a larger \tilde{k} implies that a finer grid is required to resolve the compactly supported RBF. In other words \tilde{k} is strongly related to R_p and N_u , just as M is. In the following subsection we devise a scheme via an heuristic approach to choose \tilde{k} and M . It is based on the measure of the *number of uniform grid points per partition radius*, which we denote P and is given by

$$P = \frac{N_u}{2L} R_p. \quad (45)$$

The length L of the sides of the box B is set such that all $\mathbf{y} \in \cup_i \bar{\Omega}_i$ are in B . The number of Gauss–Legendre panels $N_{\partial\Omega}$ is chosen large enough to resolve g , which in most events is sufficient to resolve $g - u^p$ as well. This is verified numerically in subsections 7.2 and 7.3.

7.1. Example 1: Parameter selection

As right hand side for (4)–(5), consider the smooth function

$$f(x, y) = -\sin(2\pi x) \sin(2\pi y), \quad (46)$$

defined in a disc centred at $(17/701, 5/439)$ with radius one. For this simple example we will study different errors and discuss how to choose parameters.

Following the approach given above we set: $L = 1.5$ and the partition radius R_p to 0.4. Thus we use 21 extension partitions and 42 zero-partitions distributed as in Figure 7. The boundary is discretised with 32 Gauss–Legendre panels. The resolution N_u varies from 40 to 500, and for each value the parameters M and \tilde{k} need to be set.

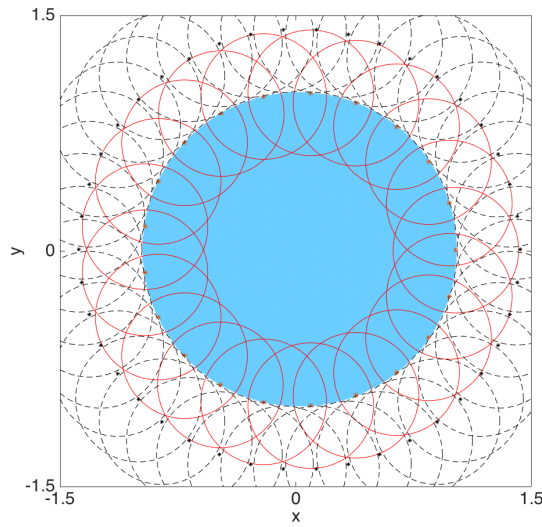


Figure 7: Regular covering of the disc Ω used in subsection 7.1. Red circles are extension partitions, black are zero-partitions. Red and black stars are centres for the extension partitions and zero partitions, respectively.

We begin by investigating the influence of the regularity of the weight function on the error convergence. To isolate this error, we want to remove the error from the local extension. Hence, instead creating an extension of f as in (37) we pick a smooth f defined in all of B and set for each interpolation patch $s_{f,\Omega_i} = f$. Only the choice of weight function, i.e. \tilde{k} , and the resolution of the uniform grid will change, the rest will be fixed.

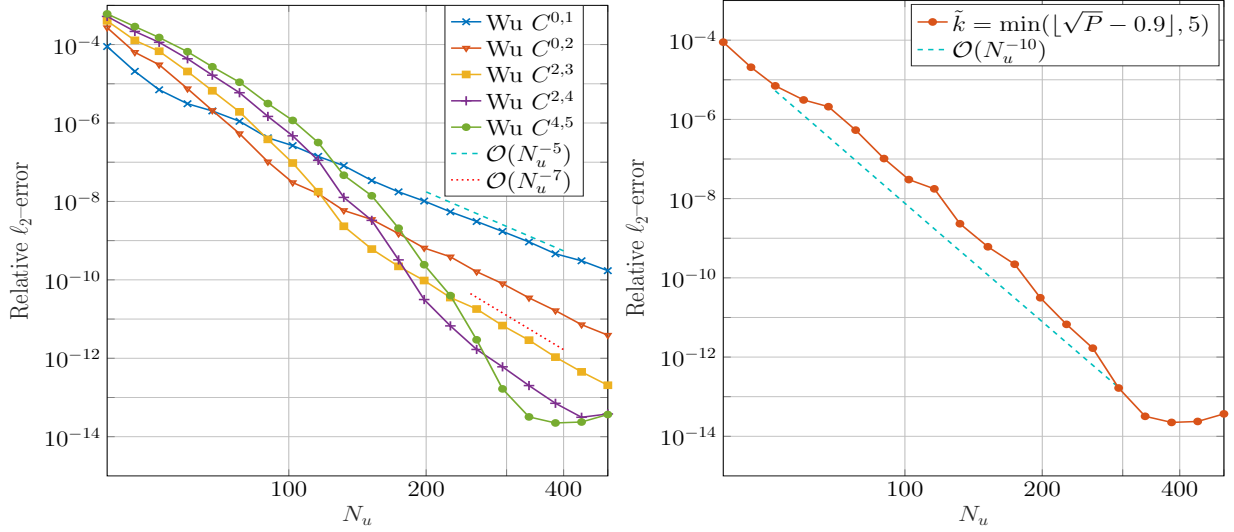


Figure 8: Error in numerical solution for the Poisson equation with right hand side given by (46), but with local extensions given by analytic expression. Left: relative ℓ_2 error as a function of N_u in loglog-scale for various compactly supported RBF given in Table 1. Right: relative ℓ_2 error as a function of N_u in loglog-scale with \tilde{k} set by (47).

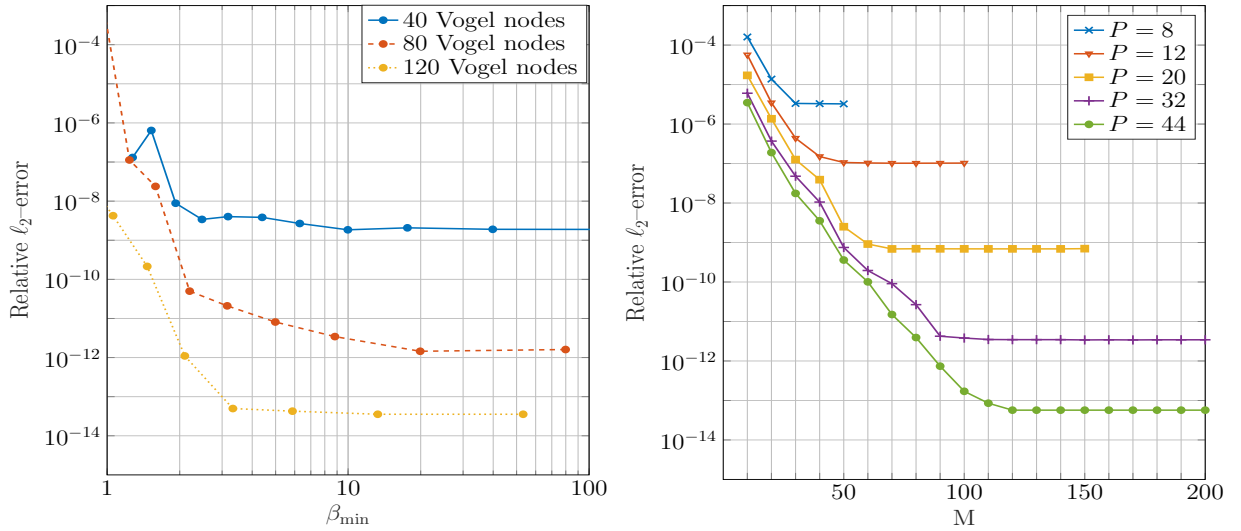


Figure 9: Error in numerical solution for the Poisson equation with f given by (46). Effect of parameter choices for computing local extension on each patch, with \tilde{k} set by (47). Left: Relative ℓ_2 error as a function of β_{\min} , defined below (44), in semilog-scale. Right: Relative ℓ_2 error as a function of number of Vogel nodes M , for different values of P (45).

In the left plot of Figure 8 the convergence of the relative ℓ_2 error is plotted in loglog-scale as a function of N_u for various compactly supported RBF used to construct w . Recall that an RBF in $C^{k,\tilde{k}}$ is of regularity k at origin and \tilde{k} at the boundary of its support. Initially the error for $C^{2,3}$ converges super algebraically and is followed by a tail with algebraic convergence, as expected. The order of convergence for the algebraic tail is inherited by the the RBFs regularity at the edge of its support. However, this is only true if we never evaluate any RBF in a neighbourhood around its origin. Compare the curves corresponding to Wu $C^{0,1}$ and Wu $C^{0,2}$ in the left plot in Figure 8. The former has an algebraic tail with slope -5 , while the latter has -6 . For Wu $C^{0,1}$ the error is dominated by the algebraic tail of order 5 for the entire spectrum of N_u . This indicates that the error associated with resolving the weights w is largest. We observe that the error for Wu function $C^{4,5}$ converges super algebraically down to a relative error of 10^{-14} , but requires a fine grid resolution to do so. First at approximately $N_u = 260$ is Wu function $C^{4,5}$ the better choice; this corresponds to $P \approx 35$. These results suggest that a higher rate of convergence can be obtained by picking an optimal RBF to construct the weight function for each N_u , compared to using the same for all N_u . Heuristically we have found that with

$$\tilde{k} = \min\left(\lfloor \sqrt{P} - 0.9 \rfloor, 5\right), \quad (47)$$

where $\lfloor x \rfloor$ gives the greatest integer less than or equal to x , we essentially obtain algebraic convergence corresponding to $O(N_u^{-10})$. This is evident from the right plot in Figure 8. Various numerical simulations confirm that the optimal choice for a given N_u is roughly the same even for different length scales and other functions f . This will be shown in subsections 7.2 and 7.3. Unless stated otherwise, in subsequent numerical experiments \tilde{k} is given by (47).

From now on we create local extension by (38), meaning M needs to be set. The left plot in Figure 9 shows the error (41) as function of β_{min} . Typically $\beta_{min} = 3$ is sufficient, and little is gained by increasing the number of data locations further. Given a fine uniform grid one can thus downsample for the interpolation problem. Solving a least squares problem is executed efficiently in MATLAB, for reference: computing $A \setminus Y$ for $A \in \mathbb{R}^{600 \times 200}$, $Y \in \mathbb{R}^{600}$ with randomised elements takes approximately 0.0054 seconds on a MacBook Pro with a 2.6 GHz Intel Core i5 processor and 16 GB of 1600 MHz DDR3 memory.

In Figure 9 the relative ℓ_2 error is plotted as a function of M for different P . Clearly the error decreases exponentially initially, but then level out around $M \approx 3P$. As safety measure we use $4P$, but note that for small N_u the resulting β_{min} may be less than three. In such case, we adjust M accordingly: the number of uniform grid points inside Ω in a given partition can be approximated by $\pi P^2/2$. To obtain a least-squares system overdetermined by at least a factor of two, M should be less than half of that, e.g. $(0.8/2)\pi P^2/2$. Thus the scheme we apply is

$$M = \min(0.8\pi P^2/4, 4P), \quad (48)$$

although a majority of numerical settings yield $M = 4P$, since $0.8\pi P^2/4 = 4P$ for $P \approx 6.4$. Note that neither (47) nor (48) are optimal, but meant as a guide to select the parameters.

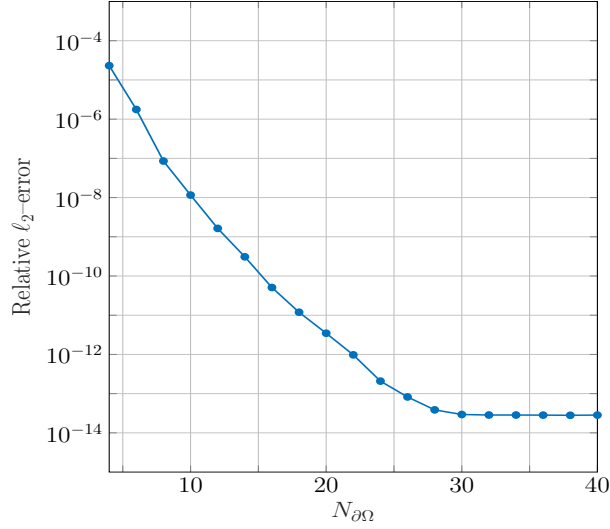


Figure 10: Relative ℓ_2 error as a function of the number of Gauss–Legendre panels $N_{\partial\Omega}$ in semilog-scale. Results are for solving the Poisson equation with f given by (46), with local extensions given by analytic expression.

In Figure 10 the relative ℓ_2 error is plotted against the number of Gauss–Legendre panels. Thus we let $N_{\partial\Omega}$ vary for $N_u = 400$ and other parameters chosen as before. Since the amount of panels sets the discrete representation for the boundary, which is used to sort points as in Ω or E , the evaluation grid is pruned. Only points considered in Ω for all the investigated resolutions are kept. We see the expected rapid convergence as the number of panels is increased.

7.2. Example 2: The Poisson equation on a multiply connected domain

We replicate the setting for the most difficult numerical experiment performed in [4], but give the details here for convenience. For this experiment we study only the error (41) as a function of N_u . We consider the right hand side

$$f(x, y) = -200 \sin(10(x + y)) + \frac{2}{9} + 1000(1000x^2 - 1)e^{-500x^2} \quad (49)$$

for the Poisson equation (4)–(5) on a complex multiply connected domain: for the outer boundary the non-zero coefficients for (43) are $c_0 = 0.25$, $d_3 = c_6 = c_8 = c_{10} = 0.01$, $c_5 = 0.02$, $R = 1$ and $n = 1$. For the inner boundary we set $c_0 = 0.05$, $c_2 = d_3 = c_5 = c_7 = 0.005$, $R = 1$ and $n = -1$.

The given right-hand side (49) exhibits steep edges parallel to the y -axis and is visualised in Figure 11. The covering consists of 38 non-zero partitions on the outer boundary and 9 partitions on the inner boundary. Different radius for the extension partitions along the outer boundary and inner boundary can be used, which requires the precomputation two different matrices A . For simplicity we let all extension matrices have the same radius, therefore they overlap more along the boundary of the cavity. The regular covering of Ω is seen in Figure 11.

For the numerical setting we let $L = 0.4$, use 64 and 44 Gauss–Legendre panels for the outer boundary and for the inner boundary, respectively. The radius for the extension partitions R_p is 0.0675. The Poisson equation is solved for grids with N_u ranging from 10^2 to 10^3 . We apply (47) and (48) to pick \tilde{k} and M . An extension f^e of (49) can be seen in Figure 11, corresponding to $N_u = 700$. The suppression to zero is rapid outside the exterior boundary of Ω and almost looks discontinuous. The extension of f into the cavity seems to mimic f remarkably well. However, a few remarks concerning the extension f^e in the cavity of Ω are in order: It is not obvious that no zero partitions are required in the cavity to obtain a well-behaved extension. Recall that far away from the boundary the extension can

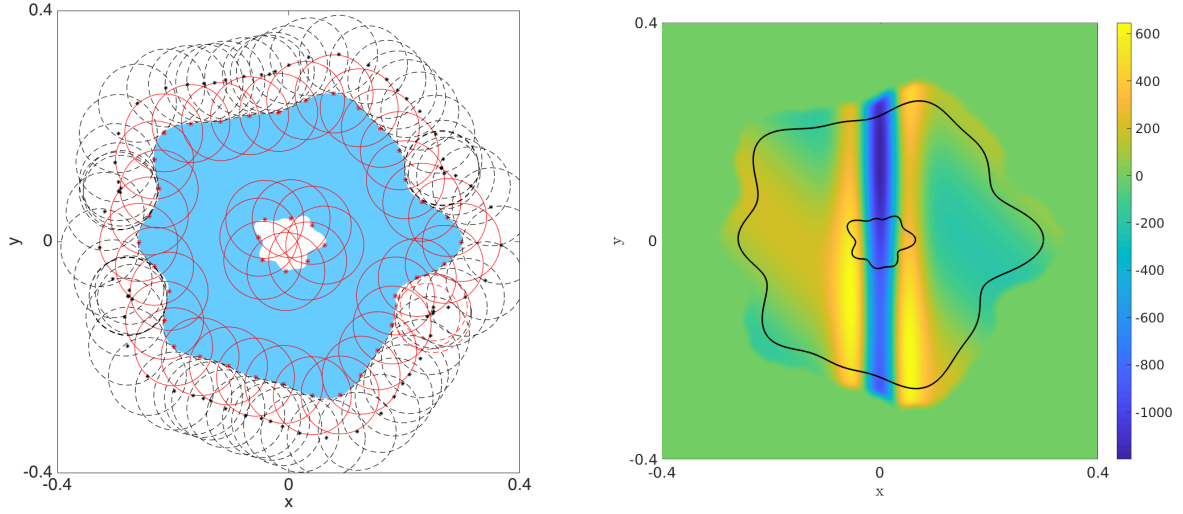


Figure 11: Left: Regular covering of Ω from subsection 7.2. Red circles are extension partitions, black are zero-partitions. Red and purple black are centres for the extension partitions and zero partitions, respectively. Right: Extension f^e by PUX of f , given by (49).

grow dramatically. This is usually an indication that smaller partitions are needed. Here we ended up with a setting where every point in the cavity belongs to an extension partition and the extension is well-behaved. Thus there is no need for zero partitions, whereas they will indeed be needed in example 3.

For the resolution $N_u = 700$ the numerical solution u and the corresponding pointwise relative error are plotted in Figure 12. In Figure 13 a convergence plot as a function of N_u is shown. As for the simpler setting we obtain an order of convergence corresponding to $O(N_u^{-10})$. This is due to the shift to a Wu function of higher regularity at suitable points as N_u increases. Thus the estimate (47) appears to be useful for more difficult numerical settings as well. For comparison, Askham et al. in [4] obtained a relative max error around 10^{-6} for an adaptive grid with in total 10^6 points with, convergence of order 3. In their embedded boundary-setting a C^0 -extension is constructed by solving the Laplace equation with f as boundary condition, as briefly explained in the introduction.

In Figure 13 the boundary condition g and modified boundary conditions $g - u^P$ are plotted, where the latter is passed as input to the integral equation solver. We observed in several simulations that $g - u^P$ is not harder to resolve than g , meaning one can choose the discretisation of $\partial\Omega$ a priori based on the originally stated boundary conditions g .

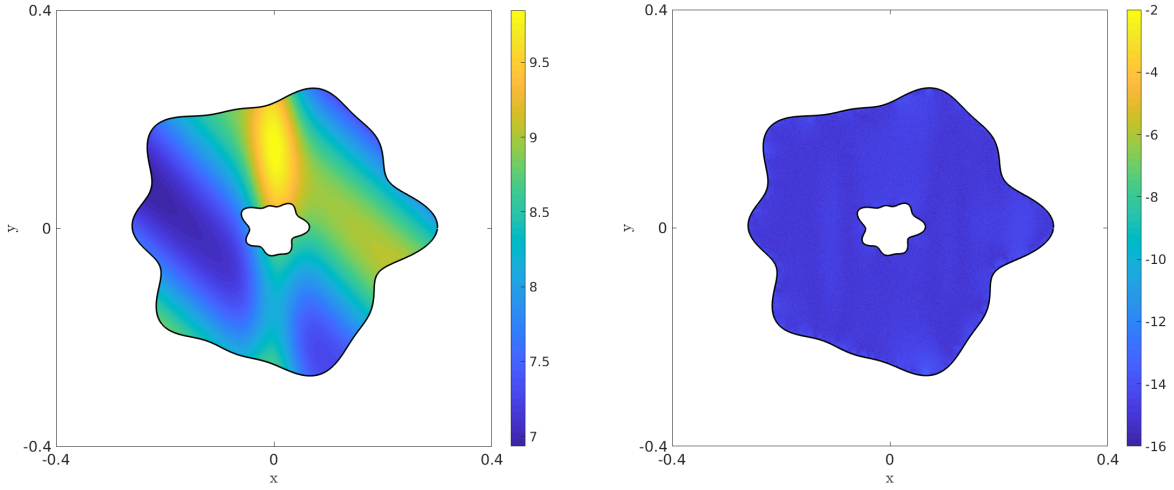


Figure 12: Left: Numerical solution u to the Poisson equation with f from (49) for $N_u = 700$. Right: Pointwise relative \log_{10} -error for $N_u = 700$. Max relative error is 3.06×10^{-13} .

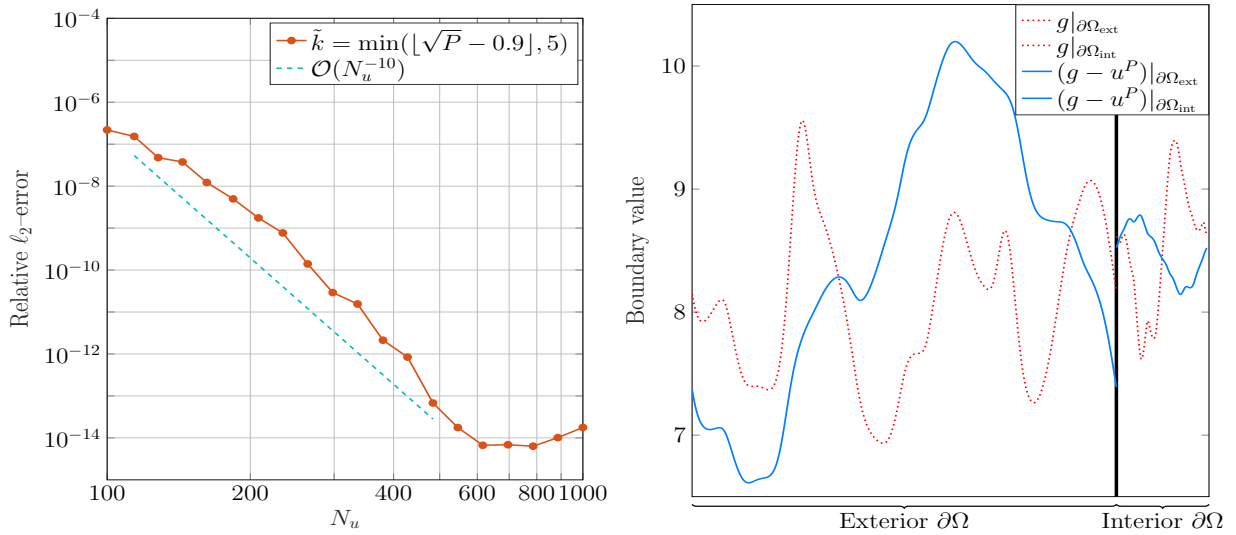


Figure 13: Results for solving the Poisson equation with (49). Left: Relative error as function of uniform grid resolution N_u , with \tilde{k} and M set by (47) and (48). Right: The boundary values g and modified boundary values $g - u^P$ on the exterior and interior boundary segments.

7.3. Example 3: The Poisson equation on a domain with a larger cavity and more oscillating right hand side

The third test features the right-hand side

$$f(x, y) = - \sum_{i=0}^5 2^{2i} e^{-\sqrt{2}^i} (\cos(2^i x) + \cos(2^i y)) \quad (50)$$

for the Poisson equation (4)–(5). It oscillates with high frequency around the boundaries and is thus overall harder to resolve than (49). The domain is again multiply connected and the non-zero coefficients for the outer boundary are $c_0 = 1$, $c_{-5} = d_{-1} = 0.2$, $R = 1$ and $n = 1$. For the inner boundary we set $c_0 = 1$, $c_{-6} = d_{-3} = 0.1$, $R = 0.3$, $b = 0.17$ and $n = -1$.

We use $L = 1.54$, 84 Gauss-Legendre panels and 82 partitions for the outer boundary and 40 Gauss-Legendre panels and 23 partitions for the inner boundary. Once again N_u ranges from 10^2 to 10^3 , \tilde{k} and M is set by (47) and (48) and all extension partitions have the same radius, $R_p = 0.12$. Consequently the partitions along the inner boundary do not cover the cavity, thus f^e must be suppressed to zero inside. See Figure 14 for f^e and the covering, which should be compared with the covering from the previous example, see Figure 11.

The numerical solution and pointwise relative error are plotted in Figure 15. The right-hand side of Figure 16 features a plot of the error (41) as a function of N_u . We observe the same trend for the convergence as in the two previous examples, but require a finer grid in this setting to reach an error of $O(10^{-14})$. This is due to (50) being harder to resolve and smaller partitions are required to obtain good approximations of the interpolants. Consequently f^e has less distance over which it goes to zero, hence a finer resolution is required to resolve it.

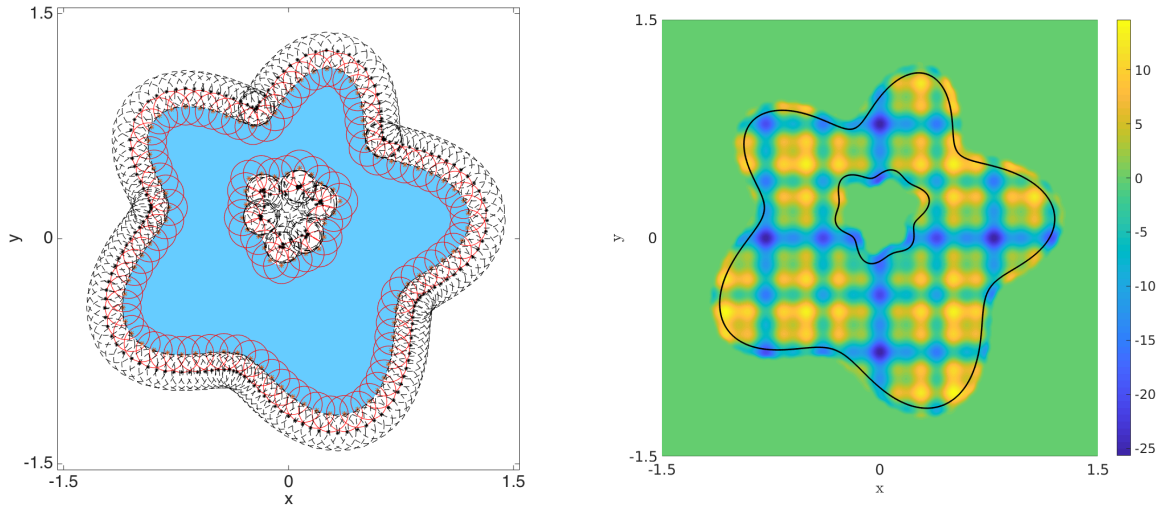


Figure 14: Left: Regular covering of Ω from subsection 7.3. Red circles are extension partitions, black are zero-partitions. Right: Extension f^e by PUX of f , given by (50).

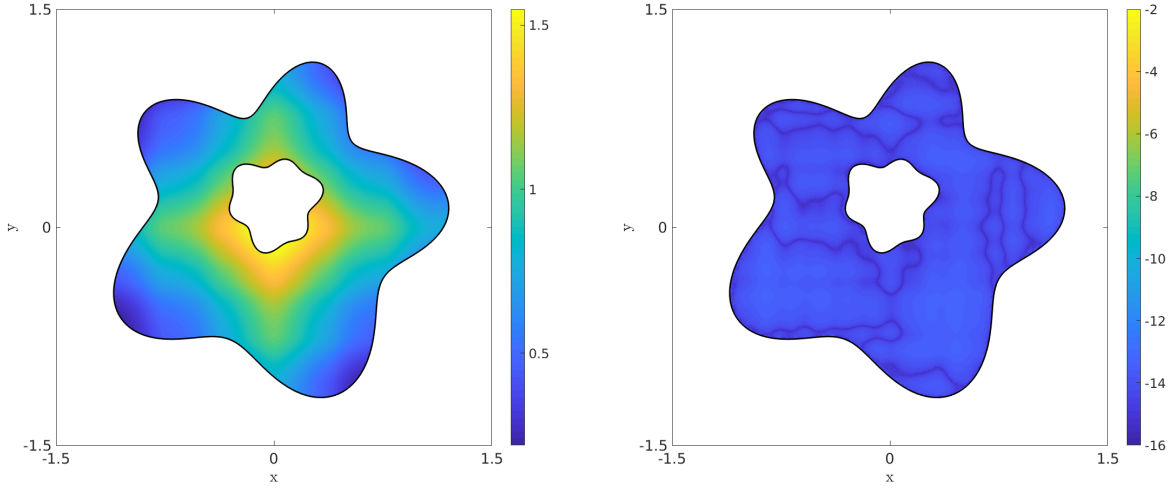


Figure 15: Left: Numerical solution u to the Poisson equation with f from (50) for $N_u = 1000$. Right: Pointwise relative \log_{10} -error for $N_u = 1000$. Max relative error is 3.53×10^{-13} .

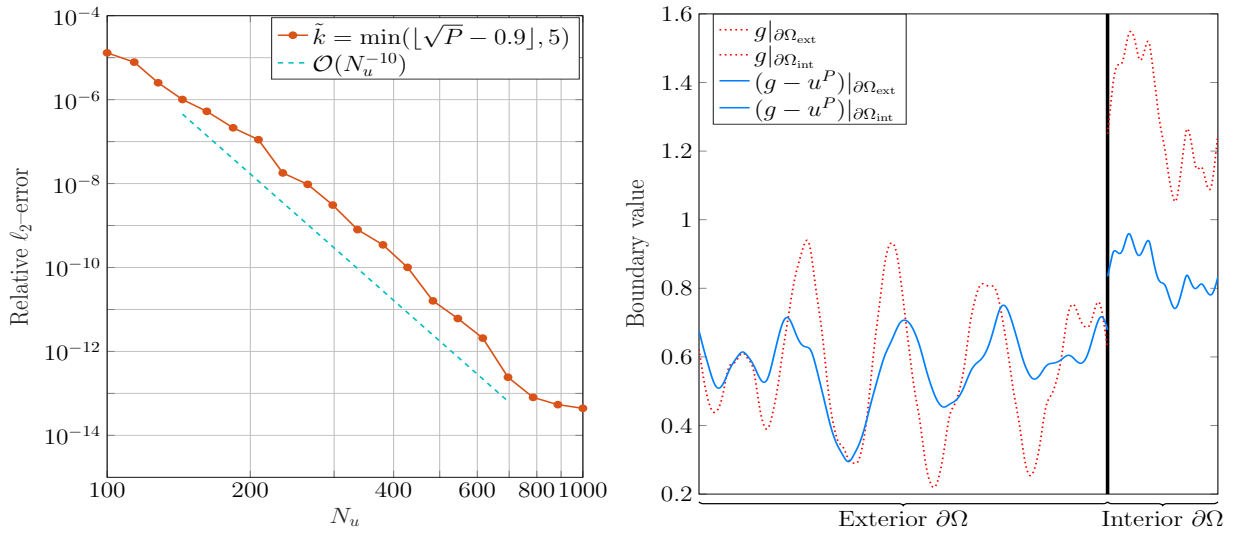


Figure 16: Results for solving the Poisson equation with right hand side given by (50). Left: Relative error as function of uniform grid resolution N_u , with \tilde{k} and M set by (47) and (48). Right: The boundary values g and modified boundary values $g - u^P$ on the exterior and interior boundary segments.

7.4. Performance and efficiency

To give an idea of the computational cost of function extension by PUX, some timings are provided in Table 2, where each time is the mean of ten runs for the numerical setting presented in subsection 7.1. Thus the number of partitions is constant, but the grid is refined, with \tilde{k} and M set thereafter. For reference we have included solving the free–space Poisson equation with the method presented in subsection 2.2. We timed:

- Building A . This is done once and the same A is reused for all extension partitions. Note that RBF–QR is used whether needed or not.
- The construction of the local extensions $\{f_i^e\}_{i=1}^{N_p}$. This includes: separating A into A_Ω and A_E as in (36), solving the least–squares problem $A_\Omega F = \tilde{F}_\Omega$ and evaluating $A_E F$ to obtain \tilde{F}_E in (37).
- Numerically evaluate f^e as in (38). For the extension partitions the precomputed values for w are reused. For the zero–partitions with radius other than R_p new evaluations are required.
- Solve for u^P . All steps are required steps are included in the timings, even the precomputation of \tilde{K} , see (22). When excluding precomputation the time is about one tenth the tabulated result.

When timing the processes above we excluded: identifying points on the uniform grid within R_p of the partition centre, identifying points as in Ω or E and precomputing the weights w .

From Table 2 we read that being able to compute A once and reuse is vital for the efficiency of PUX. Solving the least–squares problem $A_\Omega F = \tilde{F}_\Omega$, see equation (36), on each partition is the most time consuming process of constructing $\{f_i^e\}_{i=1}^{N_p}$. This is done with a QR decomposition of A_Ω and backward substitution, thus scaling as $2N_{u,i}M^2 - 2/3M^3 + N_{u,i}M$, where $N_{u,i}$ is the number of data points in partition Ω_i . However, for N_u less than 400 the local systems are not large enough for this scaling to be dominating. With downsampling to reduce β_{\min} , i.e. $N_{u,i}$, the cost of constructing $\{f_i^e\}_{i=1}^{N_p}$ is comparable to the cost of solving for u^P using an efficient FFT–based solver. Observe that in our implementation $\{f_i^e\}_{i=1}^{N_p}$ and the weights are not computed in parallel, but doing so is trivial. The cost of the RBF–QR algorithm increases with ε and the spacing between centres, both of which are comparatively large in this example. Thus these timings represent a ”worst case” scenario.

Table 2: Timings in [s] of steps for PUX and solving the free–space Poisson equation for example 7.1. Measurements are based on the mean of ten runs.

Task	$N_u = 100$	$N_u = 200$	$N_u = 400$
Build A	0.0717	0.1132	0.2852
Construct $\{f_i^e\}_{i=1}^{N_p}$	0.0078	0.0437	0.4438 ¹
Evaluate f^e	0.0043	0.0090	0.0307
Solve for u^P	0.0169	0.0611	0.2297

¹ Value for $\beta_{\min} \approx 19.2$. With downsampling to $\beta_{\min} \approx 4.8$, the corresponding time is 0.191.

8. Conclusions

In this paper, we have introduced the novel method Partition of Unity Extension, or PUX, for numerically extending a function f outside of the complex multiply connected domain it is given on. The main strength of the PUX method is that global regularity is obtained by solving local problems. This is achieved by blending local extensions on circular patches with a partition of unity function. Its regularity can be chosen and determines the global regularity. Moreover, by introducing what we call zero partitions when defining this function, a compactly supported function extension is obtained.

The performance of PUX has been thoroughly investigated by solving the Poisson equation on multiply connected complex domains. The particular solution comes from solving the free-space Poisson equation for the extended f given by PUX. Thereafter the Laplace equation is solved on the given domain using a boundary integral method, with boundary conditions modified according to the particular solution. The final solution is the sum of the two. We have demonstrated how the various parameters are related and how to set them, thereby significantly reducing the parameter space. By using these guidelines the error in the solution to the Poisson equation converges to 10^{-14} with an order of about $O(N_u^{-10})$, where $N_u \times N_u$ is the total number of uniform grid points. This shows that the method described in the paper, without any additional numerical treatment, can provide precision down to round off.

The PUX method is simple to implement, with the exception of the RBF-QR method used to compute the matrix A as defined in section 4. For this, an open-source implementation is available online [33]. The RBF-QR algorithm is computationally costly as compared to the least squares solve that follows. By centring all circular patches on a uniform grid point, the matrix A however needs to be computed only once, which yields a great reduction in the total computational cost. The local least squares problems on each patch can be solved accurately with standard methods and are typically quite small, with 100-400 unknowns.

The PUX algorithm in this paper has been designed for when the data of f is defined on a uniform grid. Generally a finer grid is required to resolve the extension as it goes to zero, compared to resolve f on Ω . Since the grid is uniform the resolution is often set by the extension. It would be possible to define the PUX method also for an adaptive grid. The implementation can be changed to allow for patches of different sizes since this is no restriction for the method.

The local extension with radial basis functions as well as the partition of unity blending naturally extends to three dimensions. Circular patches will become spherical patches, but nothing conceptually changes. A paper describing the implementation of PUX in three dimensions is forthcoming.

9. Acknowledgements

This work has been supported by the Swedish Research Council under Grant No. 2015-04998 and by the Göran Gustafsson Foundation for Research in Natural Sciences and Medicine and is gratefully acknowledged.

References

- [1] M. C. A. Kropinski, B. D. Quaife, Fast integral equation methods for the modified Helmholtz equation, *Journal of Computational Physics* 230 (2011) 425–434.
- [2] M. C. A. Kropinski, B. D. Quaife, Fast integral equation methods for Rothe’s method applied to the isotropic heat equation, *Computers and Mathematics with Applications* 61 (2011) 2436–2446.
- [3] L. Greengard, M. C. Kropinski, An integral equation approach to the incompressible Navier–Stokes equations in two dimensions, *SIAM Journal on Scientific Computing* 20 (1998) 318–336.
- [4] T. Askham, A. Cerfon, An adaptive fast multipole accelerated Poisson solver for complex geometries, *Journal of Computational Physics* 344 (2017) 1 – 22.
- [5] N. Albin, O. P. Bruno, A spectral FC solver for the compressible Navier–Stokes equations in general domains I: Explicit time-stepping, *Journal of Computational Physics* 230 (2011) 6248–6270.
- [6] D. B. Stein, R. D. Guy, B. Thomases, Immersed boundary smooth extension (ibse): A high-order method for solving incompressible flows in arbitrary smooth domains, *Journal of Computational Physics* 335 (2017) 155 – 178.
- [7] O. P. Bruno, M. Lyon, High-order unconditionally stable fc-ad solvers for general smooth domains i. basic elements, *Journal of Computational Physics* 229 (2010) 2009 – 2033.

- [8] M. Lyon, O. P. Bruno, High-order unconditionally stable fc-ad solvers for general smooth domains ii. elliptic, parabolic and hyperbolic pdes; theoretical considerations, *Journal of Computational Physics* 229 (2010) 3358 – 3381.
- [9] D. Shirokoff, J. C. Nave, A Sharp-Interface Active Penalty Method for the Incompressible Navier–Stokes Equations, *Journal of Scientific Computing* 62 (2015) 53–77.
- [10] S. H. Lui, Spectral domain embedding for elliptic PDEs in complex domains, *Journal of Computational and Applied Mathematics* 225 (2009) 541–557.
- [11] O. Bruno, M. Lyon, High-order unconditionally stable FC-AD solvers for general smooth domains I. Basic elements, *Journal of Computational Physics* 229 (2010) 2009–2033.
- [12] N. Albin, O. P. Bruno, M. Lyon, O. P. Bruno, High-order unconditionally stable FC-AD solvers for general smooth domains II. Elliptic, parabolic and hyperbolic PDEs; theoretical considerations, *Journal of Computational Physics* 229 (2010) 3358–3381.
- [13] N. Albin, O. P. Bruno, A spectral fc solver for the compressible navierstokes equations in general domains i: Explicit time-stepping, *Journal of Computational Physics* 230 (2011) 6248 – 6270.
- [14] K. Atkinson, *The Numerical Solution of Integral Equations of the Second Kind*, Cambridge Monographs on Applied and Computational Mathematics (Book 4), Cambridge University Press, 1997.
- [15] L. af Klinteberg, A. K. Tornberg, Error estimation for quadrature by expansion in layer potential evaluation, *Advances in Computational Mathematics* 43 (2017) 195–234.
- [16] J. Helsing, R. Ojala, On the evaluation of layer potentials close to their sources, *Journal of Computational Physics* 227 (2008) 2899–2921. The paper appeared electronically November 28, 2007, and subsequently in the paper issue of the journal February 20, 2008. The information about affiliations in this record was updated in December 2015. The record was previously connected to the following departments: Numerical Analysis (011015004).
- [17] A. Greenbaum, L. Greengard, G. McFadden, *Laplace’s Equation and the Dirichlet-Neumann Map in Multiply Connected Domains*, 1993.
- [18] L. Evans, *Partial Differential Equations*, Graduate studies in mathematics, American Mathematical Society, 2010.
- [19] F. Vico, L. Greengard, M. Ferrando, Fast convolution with free-space Green’s functions, *Journal of Computational Physics* 323 (2016) 191–203.
- [20] L. af Klinteberg, D. S. Shamshirgar, A.-K. Tornberg, Fast ewald summation for free-space stokes potentials, *Research in the Mathematical Sciences* 4 (2017) 1.
- [21] L. Greengard, J.-Y. Lee, Accelerating the nonuniform fast Fourier transform, *SIAM Rev.* 46 (2004) 443–454.
- [22] R. Schaback, Native hilbert spaces for radial basis functions i, in: *New Developments in Approximation Theory*, number 132 in *International Series of Numerical Mathematics*, Birkhauser Verlag, 1997, pp. 255–282.
- [23] B. Fornberg, E. Larsson, N. Flyer, Stable computations with Gaussian radial basis functions, *SIAM J. Sci. Comput.* 33 (2011) 869–892.
- [24] G. F. Fasshauer, *Meshfree Approximation Methods with MATLAB*, World Scientific Publishing Co., Inc., River Edge, NJ, USA, 2007.
- [25] H. Wendland, Error estimates for interpolation by compactly supported radial basis functions of minimal degree, *Journal of Approximation Theory* 93 (1998) 258 – 272.
- [26] E. Larsson, V. Shcherbakov, A. Heryudono, A least squares radial basis function partition of unity method for solving pdes, *SIAM Journal on Scientific Computing* (2017).
- [27] D. Shepard, A two-dimensional interpolation function for irregularly-spaced data 23 (1968) 517–524.
- [28] C. Rieger, B. Zwicknagl, Sampling inequalities for infinitely smooth functions, with applications to interpolation and machine learning, *Advances in Computational Mathematics* 32 (2009) 103–129.
- [29] E. Larsson, B. Fornberg, Theoretical and computational aspects of multivariate interpolation with increasingly flat radial basis functions, *Computers & Mathematics with Applications* 49 (2005) 103–130.
- [30] H. Wendland, Fast evaluation of radial basis functions: Methods based on partition of unity, in: *Approximation Theory X: Wavelets, Splines, and Applications*, Vanderbilt University Press, 2002, pp. 473–483.
- [31] L. Trefethen, *Spectral Methods in MATLAB*, Society for Industrial and Applied Mathematics, 2000.
- [32] L. Ying, G. Biros, D. Zorin, A high-order 3D boundary integral equation solver for elliptic PDEs in smooth domains, *Journal of Computational Physics* 219 (2006) 247–275.
- [33] E. Larsson, Radial basis function interpolation - rbf-qr, 2017. [Online; accessed 2-May-2017].